# High-spin states and signature inversion in odd-odd $^{168}$Lu

D. G. Roux,[1,2] W. C. Ma,[1,*] G. B. Hagemann,[3] D. R. Elema,[3,†] P. Fallon,[4] A. Görgen,[4,‡] B. Herskind,[3] H. Hübel,[5] J. C. Marsh,[1] G. Sletten,[3] D. Ward,[4] and J. N. Wilson[3,§]

[1]*Department of Physics and Astronomy, Mississippi State University, Mississippi State, Mississippi 39762, USA*
[2]*Department of Physics and Electronics, Rhodes University, 6140 Grahamstown, South Africa*
[3]*The Niels Bohr Institute, Blegdamsvej 17, DK-2100 Copenhagen, Denmark*
[4]*Lawrence Berkeley National Laboratory, Berkeley, California 94720, USA*
[5]*Helmholtz-Institut für Strahlen-und Kernphysik, Universität Bonn, D-53115 Bonn, Germany*

(Received 5 January 2021; accepted 17 March 2021; published 29 March 2021)

High-spin states of the odd-odd nucleus $^{168}$Lu were populated in the $^{123}$Sb($^{48}$Ca, 3n)$^{168}$Lu reaction at a beam energy of 203 MeV and decay $\gamma$ rays measured using the Gammasphere spectrometer array. The level scheme has been extended from spin 27 to 50 $\hbar$, and three new rotational bands have been added. A number of interband linking transitions were revealed, so that all but two bands could be connected with each other. High-spin band crossings, above the first $\nu i_{13/2}$ alignment, are delineated in most bands. Significant signature inversions are identified for the first time in the bands involving both favored and unfavored signatures of the $\pi h_{9/2}$ orbital, which are likely caused by a residual proton-neutron interaction. A signature inversion with small amplitude is also observed in the $\pi d_{5/2} \otimes \nu i_{13/2}$ band. Configurations are suggested for all bands based on their experimental properties, with the help of Cranked Shell Model calculations. No evidence is found for triaxial strongly deformed structures that were predicted by the calculations.

DOI: 10.1103/PhysRevC.103.034326

## I. INTRODUCTION

Odd-odd nuclei provide a wealth of nuclear structure phenomena, but experimental studies are generally challenging due to the multitude of possible combinations of quasineutrons and quasiprotons forming the band structures at low excitation energy. It is often difficult to link the low-spin states, known from $\beta$-decay studies, to high-spin structures. In such cases the excitation energies, spins, and parities of these structures cannot be determined. The $^{168}$Lu nucleus, previously studied with only a small number of detectors, drew considerable attention on account of its location on the $A \approx 160$ island of triaxial structures. The exotic wobbling excitation mode, an experimental fingerprint of nuclei with stable triaxial shape [1], was first discovered in odd lutetium ($Z = 71$) isotopes $^{163,165,167,161}$Lu [2–6] and also tantalum ($Z = 73$), $^{167}$Ta [7]. In addition, triaxial strongly deformed (TSD) rotational bands based on quasiparticle excitations (rather than the wobbling excitation) have also been identified, for example in $^{163}$Lu [8] and the odd-odd $^{164}$Lu [9]. More recently, wobbling excitations have been reported in other mass regions, such as in $^{105}$Pd [10], $^{135}$Pr [11,12], and $^{187}$Au [13].

There have been extensive theoretical studies of the topic using various approaches. Among them, early Cranked Shell Model (CSM) calculations employing the ULTIMATE CRANKER (UC) code [14,15] successfully predicted the existence of an $A \approx 160$ island of TSD structures and suggested that TSD minima with deformation parameters $(\varepsilon_2, \gamma) \approx (0.4, \pm 20^\circ)$ in the potential energy surfaces are stabilized by large single-particle shell gaps associated with proton numbers $Z = 71$ and 72 and neutron numbers $N = 94$ and 97 at large triaxiality [16–18]. The $Z = 71$ proton shell gap is clearly well established, and a neutron shell gap at $N = 94$ is supported by the observation of wobbling bands in $^{165}$Lu$_{94}$ [4] and $^{167}$Ta$_{94}$ [7]. It is thus natural to consider whether TSD structures might also exist in $^{168}$Lu, with $Z = 71$ and $N = 97$.

This work presents a detailed study of $^{168}$Lu band structures to high spins. Previously known bands, with levels below the first $\nu i_{13/2}$ alignment, are extended to high spins involving six-quasiparticle excitations. Three new bands were added after an extensive search. Quasiparticle configurations are suggested for all bands based on measured properties such as $\gamma$-ray multipolarities, $B(M1)/B(E2)$ ratios, and aligned angular momenta, in comparison with the CSM calculations as well as the systematics of nuclei in the mass region. None of the bands was found to exhibit the character of TSD structures. Significant signature inversion was observed in bands involving both the favored and unfavored signatures of the $\pi h_{9/2}$ orbital.

Section II outlines the experimental details and off-line data analysis procedures. The experimental results are presented in Sec. III. The band crossings and the configurations are discussed in Sec. IV.

*wm14@msstate.edu
†Present address: SCK CEN, BE-2400 Mol, Belgium.
‡Present address: Department of Physics, University of Oslo, N-0316 Oslo, Norway.
§Present address: IPN, F-91406 Orsay, France.

 

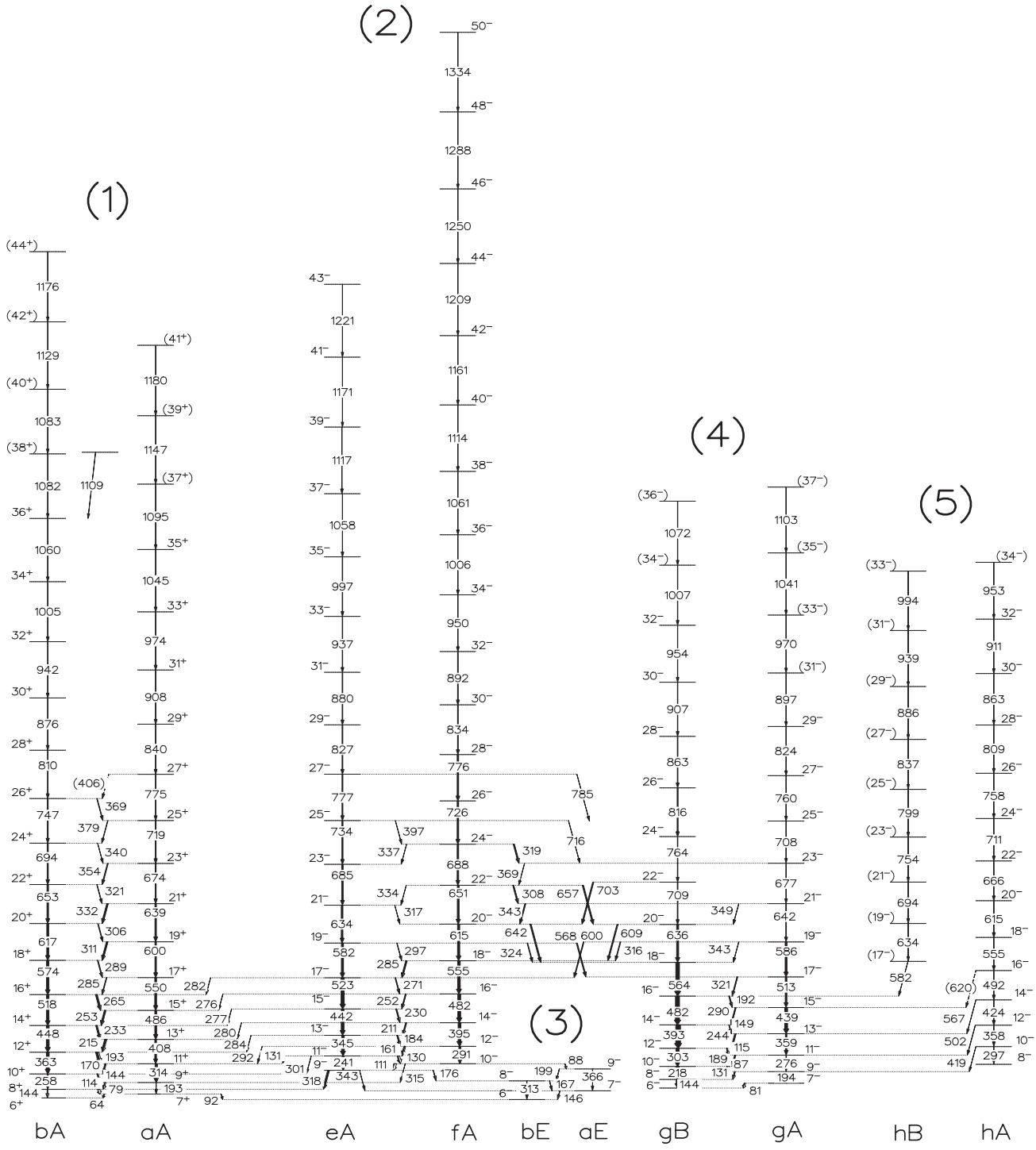


FIG. 1. Partial level scheme of $^{168}$Lu, deduced from the present data. Gamma-ray energies are in units of keV. Arrow widths indicate transition intensities. Tentative assignments are in parentheses. The labels shown below each $\gamma$-ray sequence represent the proposed quasiparticle configurations that will be discussed in Sec. IV.

## II. EXPERIMENTAL DETAILS

High-spin states of $^{168}$Lu nuclei were populated via the $^{123}$Sb($^{48}$Ca, $3n$) reaction with a beam energy of 203 MeV, using the 88″ cyclotron at Lawrence Berkeley National Laboratory. The target consists of two stacked 520 $\mu$g/cm$^2$ self-supporting foils enriched to 97.7% in $^{123}$Sb. At this energy the dominant residuals $^{167}$Lu (from the $4n$ channel) and $^{168}$Lu were populated in the approximate ratio 5 : 2. Coincident $\gamma$ rays were measured using the Gammasphere spectrometer array [19] (comprising 100 Compton-suppressed Ge detectors in this experiment), and a data set of approximately $2.2 \times 10^9$ fivefold (or higher) coincidence events was collected. The data

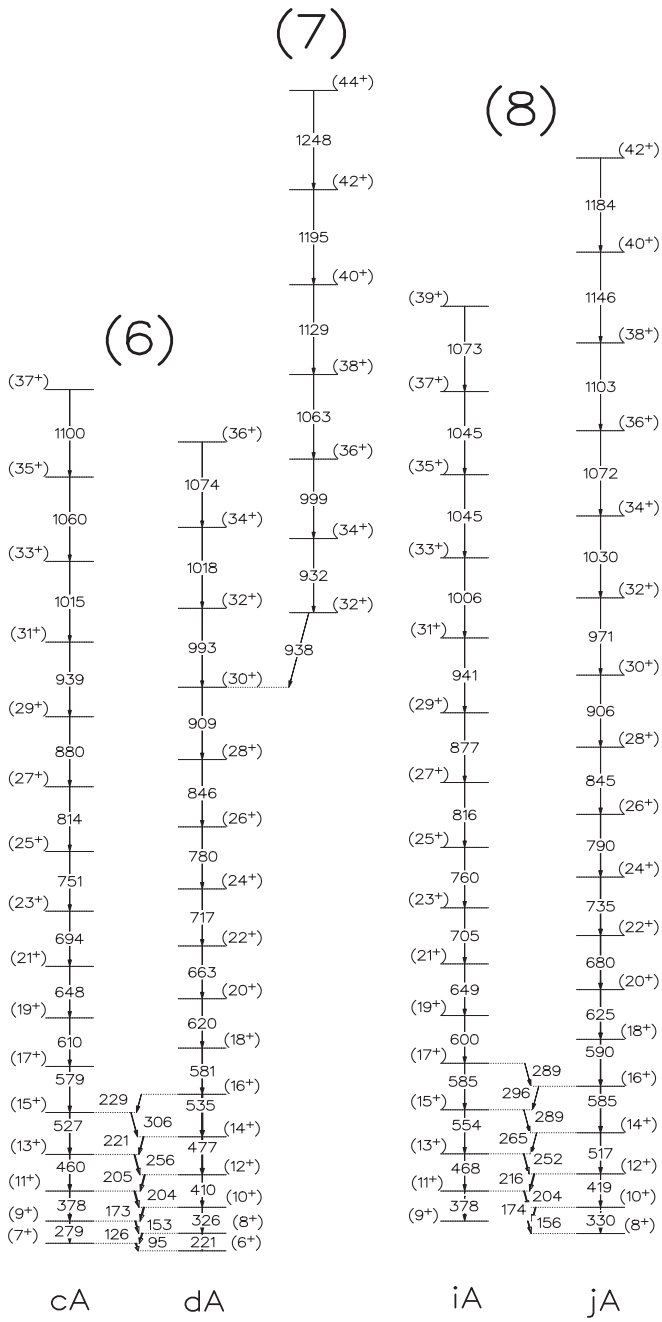


FIG. 2. Partial level scheme of $^{168}$Lu (continued from Fig. 1).

led to the identification of the wobbling excitation in $^{167}$Lu [5], which formed part of a more complete spectroscopic study [20]. The current spectroscopy of $^{168}$Lu is based on the same data set.

In the off-line analysis the RADWARE software package [21] was used to construct three-dimensional (cube) and four-dimensional (hypercube) histograms, and to then analyze the $\gamma$-ray coincidence relationships. The RADWARE band search routine was used extensively to look for weak bands. In addition, an analysis of $\gamma$-ray directional correlation from oriented states (DCO ratios) [22] was performed to determine the multipolarity of the $\gamma$ rays. Gated DCO matrices, with detectors at 32°, 37°, 143°, 148° and 163° along the $x$ axis, and detectors from 58° through 122° along the $y$ axis, were constructed for each $\gamma$-ray sequence. The extracted DCO ratios of $\gamma$-ray transitions from stretched quadrupole gated spectra fall into two distinct groups centered around 1.0 and 0.6 for stretched quadrupole and dipole transitions, respectively. The mixed $M1/E2$ transitions in the coupled bands usually have DCO ratios between 0.6 and 1.0, depending on mixing ratios. A more detailed analysis for expected DCO ratios of various $\gamma$ rays under different gating conditions was presented in a previous publication [23]. The parity assignments are based on the multipolarities of linking transitions between bands, as well as on coincidence relationships that introduce important constraints in some instances. Spins for the highest lying transitions were assigned by assuming a consistent rotational behavior when DCO ratios could not be measured.

## III. LEVEL SCHEME

Excited states of $^{168}$Lu were previously studied by several groups using the $^{159}$Tb($^{13}$C, 4$n$) [24] and $^{154}$Sm($^{19}$F, 5$n$) [25,26] reactions. Four coupled bands, labeled as Bands 1, 2, 4, and 6 in Figs. 1 and 2, were measured up to spins 27$\hbar$, and interpreted as an $i_{13/2}$, $\nu[642]5/2^+$ quasineutron coupled, respectively, with $\pi[404]7/2^+$, $\pi[514]9/2^-$, $\pi[541]1/2^-$, and $\pi[402]5/2^+$ quasiproton orbitals. A low-spin structure, Band 3, was also established [26], linked with Bands 1 and 2, and associated with a $\pi[404]7/2^+ \otimes \nu[523]5/2^-$ configuration built on the previously identified $6^-$ ground state [27,28].

The level scheme has now been extended to significantly higher spins. For example, Bands 1 and 2 were observed from spins 27 and 23 to (44) and 50, respectively. Three new bands, Bands 5, 7, and 8, were observed for the first time. Extensive cross-talk between Bands 4 and 2, and decays from Band 5 to Band 4 were identified. Band 7 is a short high-spin sequence feeding Band 6. However, the linking from Bands 6 and 8 to the rest of the level scheme has not been established. The $\gamma$-ray transition energies, intensities, level energies, spin and parity assignments, as well as DCO ratios, are listed in Table I.

### A. Bands 1–5

Band 1 is linked directly to the $6^-$ ground state via a 92-keV ($7^+ \rightarrow 6^-$) transition [24,26]. Its DCO ratio, 0.55(7), is consistent with a pure dipole nature, most likely an $E1$, rather than a $M1/E2$ mixed transition. The lower part of the band is fed by a number of $E1$ transitions from Band 2. Two of them, 318 ($9^- \rightarrow 8^+$) and 315 keV ($10^- \rightarrow 9^+$), were observed previously [26]. Seven new stretched $E1$ transitions have been revealed up to the state $17^-$ in Band 2, together with a 131-keV $11^- \rightarrow 11^+$ transition. The decay sequence with odd-spins ($\alpha = 1$) has been extended from $I = 27$ to (41), and the even-spins ($\alpha = 0$) from 26 to (44). The coincidence spectra for the high-spin region of Band 1 are displayed in Fig. 3, while the spectra of the lower-spin region can be seen in the previous publication [24].

Two previously identified depopulating transitions, 176 ($9^- \rightarrow 8^-$) and 343 keV ($9^- \rightarrow 7^-$) from Band 2 to Band 3 [26], have been confirmed in the current work. Another link-

TABLE I. $\gamma$-ray energies $E_\gamma$ (in keV), suggested spins and parities of the initial ($I_i^\pi$) and final ($I_f^\pi$) states, excitation energies $E_i$ (in keV) of initial states, DCO ratios, and for interband linking transitions the band number ($N$) of the final states. Relative intensities ($I_\gamma$) are normalized to the 393.1-keV ($14^- \rightarrow 12^-$) transition ($\equiv 1000$) in Band 4.

| $E_\gamma$[a] | $I_i^\pi \rightarrow I_f^\pi$[b] | $E_i$ | DCO | $I_\gamma$ | N |
|---|---|---|---|---|---|
| **Band 1** | | | | | |
| | $6^+$ | 27.2 | | | |
| 91.6 | $7^+ \rightarrow 6^-$ | 91.6 | 0.55(7) | 8(3) | 3 |
| 64.4 | $7^+ \rightarrow 6^+$ | | 0.64(4) | 10(3) | |
| 143.6 | $8^+ \rightarrow 6^+$ | 170.8 | 0.99(1) | $\leqslant 3$ | |
| 79.3 | $8^+ \rightarrow 7^+$ | | 0.75(6) | 9(3) | |
| 193.2 | $9^+ \rightarrow 7^+$ | 284.8 | | 55(5) | |
| 113.9 | $9^+ \rightarrow 8^+$ | | 0.81(3) | 67(8) | |
| 258.2 | $10^+ \rightarrow 8^+$ | 429.0 | 0.96(4) | 312(11) | |
| 144.2 | $10^+ \rightarrow 9^+$ | | 0.81(3) | 190(7) | |
| 314.4 | $11^+ \rightarrow 9^+$ | 599.2 | 0.99(4) | 281(15) | |
| 170.2 | $11^+ \rightarrow 10^+$ | | 0.83(6) | 69(4) | |
| 363.2 | $12^+ \rightarrow 10^+$ | 792.3 | 1.06(4) | 540(16) | |
| 193.0 | $12^+ \rightarrow 11^+$ | | 0.64(5) | 80(9) | |
| 408.2 | $13^+ \rightarrow 11^+$ | 1007.4 | 1.00(4) | 427(22) | |
| 215.2 | $13^+ \rightarrow 12^+$ | | 0.64(7) | 67(10) | |
| 447.9 | $14^+ \rightarrow 12^+$ | 1240.3 | 1.06(4) | 582(17) | |
| 232.8 | $14^+ \rightarrow 13^+$ | | 0.79(8) | 66(3) | |
| 486.0 | $15^+ \rightarrow 13^+$ | 1493.3 | 0.98(8) | 496(26) | |
| 253.0 | $15^+ \rightarrow 14^+$ | | 0.82(12) | 52(3) | |
| 517.8 | $16^+ \rightarrow 14^+$ | 1758.2 | 1.05(4) | 530(30) | |
| 264.9 | $16^+ \rightarrow 15^+$ | | 0.76(8) | 43(3) | |
| 549.9 | $17^+ \rightarrow 15^+$ | 2043.0 | 0.99(5) | 452(24) | |
| 284.7 | $17^+ \rightarrow 16^+$ | | 0.65(6) | 38(2) | |
| 573.7 | $18^+ \rightarrow 16^+$ | 2332.2 | 1.04(4) | 472(27) | |
| 289.2 | $18^+ \rightarrow 17^+$ | | 0.81(8) | 73(4) | |
| 600.0 | $19^+ \rightarrow 17^+$ | 2642.9 | 1.06(4) | 375(20) | |
| 310.7 | $19^+ \rightarrow 18^+$ | | 0.63(9) | 36(2) | |
| 616.8 | $20^+ \rightarrow 18^+$ | 2949.0 | 1.01(4) | 407(24) | |
| 306.2 | $20^+ \rightarrow 19^+$ | | 0.68(7) | 43(3) | |
| 638.6 | $21^+ \rightarrow 19^+$ | 3281.5 | 0.97(4) | 273(15) | |
| 332.4 | $21^+ \rightarrow 20^+$ | | 0.68(10) | 32(2) | |
| 653.2 | $22^+ \rightarrow 20^+$ | 3602.2 | 1.02(4) | 339(20) | |
| 320.7 | $22^+ \rightarrow 21^+$ | | 0.76(11) | 33(2) | |
| 674.1 | $23^+ \rightarrow 21^+$ | 3955.8 | 0.98(4) | 208(12) | |
| 353.7 | $23^+ \rightarrow 22^+$ | | 0.75(11) | 23(1) | |
| 694.4 | $24^+ \rightarrow 22^+$ | 4295.9 | 1.02(4) | 245(15) | |
| 340.0 | $24^+ \rightarrow 23^+$ | | 0.72(11) | 17(4) | |
| 718.7 | $25^+ \rightarrow 23^+$ | 4674.4 | 1.06(4) | 160(10) | |
| 378.6 | $25^+ \rightarrow 24^+$ | | 0.58(9) | 15(1) | |
| 747.2 | $26^+ \rightarrow 24^+$ | 5043.1 | 1.02(4) | 166(10) | |
| 368.7 | $26^+ \rightarrow 25^+$ | | 0.66(13) | 13(1) | |
| 775.4 | $27^+ \rightarrow 25^+$ | 5449.3 | 0.94(5) | 118(7) | |
| 406.1 | $27^+ \rightarrow 26^+$ | | | $\leqslant 3$ | |
| 809.6 | $28^+ \rightarrow 26^+$ | 5852.7 | 1.02(4) | 114(8) | |
| 840.2 | $29^+ \rightarrow 27^+$ | 6289.5 | 1.01(10) | 64(4) | |
| 876.1 | $30^+ \rightarrow 28^+$ | 6728.8 | 1.00(5) | 73(5) | |
| 907.7 | $31^+ \rightarrow 29^+$ | 7197.2 | 1.05(16) | 48(3) | |
| 942.4 | $32^+ \rightarrow 30^+$ | 7671.3 | 1.02(10) | 54(2) | |
| 974.0 | $33^+ \rightarrow 31^+$ | 8171.2 | 1.06(16) | 30(2) | |
| 1005.3 | $34^+ \rightarrow 32^+$ | 8676.6 | 0.98(15) | 36(2) | |
| 1044.7 | $35^+ \rightarrow 33^+$ | 9215.9 | 1.09(22) | 13(2) | |
| 1059.6 | $36^+ \rightarrow 34^+$ | 9736.2 | 1.01(15) | 25(2) | |
| 1095.3 | $(37^+) \rightarrow 35^+$ | 10311.2 | | 7(1) | |
| 1082.0 | $(38^+) \rightarrow 36^+$ | 10818.2 | | $\approx$6(2)[c] | |
| 1109.1 | $\rightarrow 36^+$ | 10845.3 | | 8(2) | |
| 1146.6 | $(39^+) \rightarrow (37^+)$ | 11457.8 | | 3(1) | |
| 1083.0 | $(40^+) \rightarrow (38^+)$ | 11901.2 | | $\approx$4(2)[c] | |
| 1180.1 | $(41^+) \rightarrow (39^+)$ | 12637.9 | | $\leqslant 3$ | |
| 1129.0 | $(42^+) \rightarrow (40^+)$ | 13030.2 | | $\leqslant 3$ | |
| 1176.0 | $(44^+) \rightarrow (42^+)$ | 14206.2 | | $\leqslant 3$ | |
| **Band 2** | | | | | |
| 318.2 | $9^- \rightarrow 8^+$ | 489.0 | | $\approx$30(6)[c] | 1 |
| 342.7 | $9^- \rightarrow 7^-$ | | | 33(6)[c] | 3 |
| 176.0 | $9^- \rightarrow 8^-$ | | 0.72(5) | 15(3) | 3 |
| 111.0 | $10^- \rightarrow 9^-$ | 600.0 | | 25(5) | |
| 315.2 | $10^- \rightarrow 9^+$ | | | 35(9) | 1 |
| 87.7 | $10^- \rightarrow 9^-$ | | | $\leqslant 3$ | 3 |
| 241.4 | $11^- \rightarrow 9^-$ | 730.5 | 0.94(19) | 29(5) | |
| 130.4 | $11^- \rightarrow 10^-$ | | 0.75(4) | 148(18) | |
| 301.4 | $11^- \rightarrow 10^+$ | | 0.70(14) | 28(7) | 1 |
| 131.3 | $11^- \rightarrow 11^+$ | | 1.07(16) | $\leqslant 3$ | 1 |
| 291.4 | $12^- \rightarrow 10^-$ | 891.5 | 0.99(15) | 50(6) | |
| 161.0 | $12^- \rightarrow 11^-$ | | 0.79(4) | 104(8) | |
| 292.3 | $12^- \rightarrow 11^+$ | | 0.83(12) | $\leqslant 3$ | 1 |
| 345.0 | $13^- \rightarrow 11^-$ | 1075.8 | 0.97(4) | 300(36) | |
| 184.3 | $13^- \rightarrow 12^-$ | | 0.74(3) | 237(31) | |
| 283.6 | $13^- \rightarrow 12^+$ | | 0.71(7) | 25(8) | 1 |
| 395.2 | $14^- \rightarrow 12^-$ | 1287.0 | 0.92(9) | 306(38) | |
| 211.2 | $14^- \rightarrow 13^-$ | | 0.71(7) | 281(37) | |
| 279.6 | $14^- \rightarrow 13^+$ | | 0.73(15) | 16(4) | 1 |
| 441.8 | $15^- \rightarrow 13^-$ | 1517.5 | 1.02(4) | 363(43) | |
| 230.4 | $15^- \rightarrow 14^-$ | | 0.74(3) | 215(26) | |
| 277.2 | $15^- \rightarrow 14^+$ | | 0.83(17) | 16(6) | 1 |
| 482.4 | $16^- \rightarrow 14^-$ | 1769.5 | 0.95(5) | 297(53) | |
| 252.0 | $16^- \rightarrow 15^-$ | | 0.65(4) | 182(40) | |
| 276.2 | $16^- \rightarrow 15^+$ | | | 4(1) | 1 |
| 522.7 | $17^- \rightarrow 15^-$ | 2040.2 | 1.06(4) | 460(57) | |
| 270.7 | $17^- \rightarrow 16^-$ | | 0.63(3) | 191(24) | |
| 282.0 | $17^- \rightarrow 16^+$ | | | $\leqslant 3$ | 1 |
| 555.4 | $18^- \rightarrow 16^-$ | 2324.8 | 1.04(5) | 461(67) | |
| 284.6 | $18^- \rightarrow 17^-$ | | 0.59(5) | 251(82) | |
| 581.8 | $19^- \rightarrow 17^-$ | 2622.0 | 1.01(4) | 602(70) | |
| 297.2 | $19^- \rightarrow 18^-$ | | 0.76(11) | 49(9) | |
| 567.9 | $19^- \rightarrow 17^-$ | | 0.95(7) | 46(9) | 4 |
| 324.2 | $19^- \rightarrow 18^-$ | | 0.69(10) | 24(3) | 4 |
| 614.6 | $20^- \rightarrow 18^-$ | 2939.4 | 1.00(10) | 220(38) | |
| 641.6 | $20^- \rightarrow 18^-$ | | 1.04(10) | 266(53) | 4 |
| 634.4 | $21^- \rightarrow 19^-$ | 3256.4 | 1.04(4) | 372(65) | |
| 317.0 | $21^- \rightarrow 20^-$ | | | $\approx$12(4)[c] | |
| 650.8 | $22^- \rightarrow 20^-$ | 3590.2 | 0.94(9) | 123(21) | |
| 333.8 | $22^- \rightarrow 21^-$ | | | 21(6) | |
| 656.8 | $22^- \rightarrow 20^-$ | | 1.00(4) | 194(34) | 4 |
| 308.1 | $22^- \rightarrow 21^-$ | | 0.61(9) | 116(22) | 4 |
| 684.6 | $23^- \rightarrow 21^-$ | 3941.0 | 0.97(4) | 355(66) | |
| 687.8 | $24^- \rightarrow 22^-$ | 4277.9 | 0.91(9) | 260(38) | |
| 336.9 | $24^- \rightarrow 23^-$ | | | 33(6) | |
| 319.0 | $24^- \rightarrow 23^-$ | | 0.77(8) | 104(16) | 4 |
| 733.6 | $25^- \rightarrow 23^-$ | 4674.6 | 1.01(10) | 193(38) | |

TABLE I. (*Continued.*)

| $E_\gamma$[a] | $I_i^\pi \rightarrow I_f^\pi$[b] | $E_i$ | DCO | $I_\gamma$ | N |
|---|---|---|---|---|---|
| 396.7 | $25^- \rightarrow 24^-$ | | | $\leqslant 3$ | |
| 715.7 | $25^- \rightarrow 23^-$ | | | 74(17) | 4 |
| 725.8 | $26^- \rightarrow 24^-$ | 5003.7 | 1.06(11) | 116(23) | |
| 776.6 | $27^- \rightarrow 25^-$ | 5451.2 | 1.05(11) | 143(29) | |
| 784.4 | $27^- \rightarrow (25^-)$ | | 0.98(20) | 28(7) | 4 |
| 776.2 | $28^- \rightarrow 26^-$ | 5779.9 | 0.92(9) | 107(22) | |
| 826.9 | $29^- \rightarrow 27^-$ | 6278.1 | 1.01(15) | 100(21) | |
| 833.9 | $30^- \rightarrow 28^-$ | 6613.8 | 1.00(10) | 95(19) | |
| 880.4 | $31^- \rightarrow 29^-$ | 7158.6 | 0.99(15) | 55(12) | |
| 892.4 | $32^- \rightarrow 30^-$ | 7506.3 | 0.94(20) | 76(18) | |
| 936.8 | $33^- \rightarrow 31^-$ | 8095.4 | 0.90(14) | 38(8) | |
| 950.2 | $34^- \rightarrow 32^-$ | 8456.5 | 0.96(14) | 56(15) | |
| 997.4 | $35^- \rightarrow 33^-$ | 9092.8 | 1.04(21) | 24(5) | |
| 1006.4 | $36^- \rightarrow 34^-$ | 9463.0 | 1.06(16) | 49(14) | |
| 1058.0 | $37^- \rightarrow 35^-$ | 10150.8 | 1.11(24) | 21(4) | |
| 1061.2 | $38^- \rightarrow 36^-$ | 10524.2 | 1.10(23) | 32(9) | |
| 1116.8 | $39^- \rightarrow 37^-$ | 11267.6 | 1.02(22) | 12(3) | |
| 1113.9 | $40^- \rightarrow 38^-$ | 11638.1 | 1.02(20) | 19(5) | |
| 1171.2 | $41^- \rightarrow 39^-$ | 12438.8 | 1.29(26) | 6(2) | |
| 1161.4 | $42^- \rightarrow 40^-$ | 12799.5 | 1.17(25) | 13(3) | |
| 1220.8 | $43^- \rightarrow 41^-$ | 13659.6 | 1.34(27) | 4(2) | |
| 1209.0 | $44^- \rightarrow 42^-$ | 14008.5 | 1.38(28) | 7(2) | |
| 1250.3 | $46^- \rightarrow 44^-$ | 15257.6 | 1.35(27) | 5(2) | |
| 1287.7 | $48^- \rightarrow 46^-$ | 16548.3 | 1.07(21) | $\leqslant 3$ | |
| 1333.5 | $50^- \rightarrow 48^-$ | 17881.8 | 1.05(21) | $\leqslant 3$ | |
| **Band 3** | | | | | |
| | $6^-$ | 0.0 | | | |
| 146.3 | $7^- \rightarrow 6^-$ | 146.3 | | $\leqslant 3$ | |
| 313.0 | $8^- \rightarrow 6^-$ | 313.0 | | $\leqslant 3$ | |
| 166.7 | $8^- \rightarrow 7^-$ | | | $\leqslant 3$ | |
| 366.0 | $9^- \rightarrow 7^-$ | 512.3 | | $\leqslant 3$ | |
| 199.3 | $9^- \rightarrow 8^-$ | | | $\leqslant 3$ | |
| **Band 4** | | | | | |
| | $6^-$ | 192.1 | | | |
| 81.1 | $7^- \rightarrow 6^-$ | 273.2 | | $\leqslant 3$ | |
| 144.4 | $8^- \rightarrow 6^-$ | 336.5 | 0.97(10) | 52(11) | |
| 63.1 | $8^- \rightarrow 7^-$ | | | $\leqslant 3$ | |
| 194.4 | $9^- \rightarrow 7^-$ | 467.6 | 1.09(16) | 227(7) | |
| 131.0 | $9^- \rightarrow 8^-$ | | 0.70(4) | 254(20) | |
| 218.0 | $10^- \rightarrow 8^-$ | 554.7 | 0.99(7) | 335(34) | |
| 87.1 | $10^- \rightarrow 9^-$ | | | $\leqslant 3$ | |
| 276.0 | $11^- \rightarrow 9^-$ | 743.3 | 0.92(4) | 363(21) | |
| 188.6 | $11^- \rightarrow 10^-$ | | 0.60(5) | 303(22) | |
| 303.2 | $12^- \rightarrow 10^-$ | 858.2 | 1.01(4) | 756(76) | |
| 114.9 | $12^- \rightarrow 11^-$ | | 0.62(4) | 70(9) | |
| 358.9 | $13^- \rightarrow 11^-$ | 1102.5 | 0.96(5) | 381(21) | |
| 244.3 | $13^- \rightarrow 12^-$ | | 0.71(3) | 187(14) | |
| 393.1 | $14^- \rightarrow 12^-$ | 1251.2 | 1.03(4) | 1000 (1) | |
| 148.8 | $14^- \rightarrow 13^-$ | | 0.75(11) | 28(1) | |
| 438.8 | $15^- \rightarrow 13^-$ | 1541.3 | 1.00(4) | 507(27) | |
| 290.0 | $15^- \rightarrow 14^-$ | | 0.71(3) | 227(19) | |
| 481.7 | $16^- \rightarrow 14^-$ | 1733.0 | 1.01(4) | 908(30) | |
| 191.7 | $16^- \rightarrow 15^-$ | | 0.70(14) | 62(3) | |
| 513.1 | $17^- \rightarrow 15^-$ | 2054.1 | 0.96(4) | 478(26) | |
| 321.2 | $17^- \rightarrow 16^-$ | | 0.64(3) | 136(12) | |
| 564.3 | $18^- \rightarrow 16^-$ | 2297.8 | 0.96(4) | 823(34) | |
| 586.0 | $19^- \rightarrow 17^-$ | 2640.6 | 0.92(4) | 287(30) | |

TABLE I. (*Continued.*)

| $E_\gamma$[a] | $I_i^\pi \rightarrow I_f^\pi$[b] | $E_i$ | DCO | $I_\gamma$ | N |
|---|---|---|---|---|---|
| 342.8 | $19^- \rightarrow 18^-$ | | 0.61(12) | 68(4) | |
| 600.4 | $19^- \rightarrow 17^-$ | | 1.08(6) | 141(24) | 2 |
| 315.8 | $19^- \rightarrow 18^-$ | | 0.77(8) | ≈180(28)[c] | 2 |
| 636.4 | $20^- \rightarrow 18^-$ | 2933.4 | 0.52(7) | 443(14) | |
| 608.6 | $20^- \rightarrow 18^-$ | | 0.98(10) | 342(26) | 2 |
| 641.6 | $21^- \rightarrow 19^-$ | 3282.1 | 0.97(4) | 265(28) | |
| 348.8 | $21^- \rightarrow 20^-$ | | 0.66(13) | 54(9) | |
| 342.7 | $21^- \rightarrow 20^-$ | | 0.79(10) | ≈117(14)[c] | 2 |
| 709.1 | $22^- \rightarrow 20^-$ | 3642.3 | 0.97(4) | 266(14) | |
| 702.9 | $22^- \rightarrow 20^-$ | | 1.07(5) | 319(30) | 2 |
| 676.8 | $23^- \rightarrow 21^-$ | 3958.9 | 1.00(15) | 173(19) | |
| 368.7 | $23^- \rightarrow 22^-$ | | 0.72(14) | 12(2) | 2 |
| 763.7 | $24^- \rightarrow 22^-$ | 4406.0 | 1.00(10) | 144(8) | |
| 707.5 | $25^- \rightarrow 23^-$ | 4666.4 | 0.90(18) | 29(4) | |
| 816.0 | $26^- \rightarrow 24^-$ | 5222.0 | 0.99(15) | 63(7) | |
| 760.4 | $27^- \rightarrow 25^-$ | 5426.8 | 1.05(21) | 11(2) | |
| 863.1 | $28^- \rightarrow 26^-$ | 6085.1 | 0.95(14) | 44(5) | |
| 823.5 | $29^- \rightarrow 27^-$ | 6250.3 | 0.97(19) | 10(2) | |
| 907.0 | $30^- \rightarrow 28^-$ | 6992.1 | 1.20(24) | 22(3) | |
| 896.6 | $(31^-) \rightarrow 29^-$ | 7146.9 | | 9(2) | |
| 954.3 | $32^- \rightarrow 30^-$ | 7946.4 | 1.09(22) | 12(2) | |
| 970.4 | $(33^-) \rightarrow (31^-)$ | 8117.4 | | $\leqslant 3$ | |
| 1007.1 | $(34^-) \rightarrow 32^-$ | 8953.5 | 1.36(27) | 8(1) | |
| 1041.3 | $(35^-) \rightarrow (33^-)$ | 9158.7 | | $\leqslant 3$ | |
| 1072.4 | $(36^-) \rightarrow (34^-)$ | 10025.9 | 1.20(24) | 4(1) | |
| 1103.4 | $(37^-) \rightarrow (35^-)$ | 10262.1 | | $\leqslant 3$ | |
| **Band 5** | | | | | |
| | $8^-$ | 590.1 | | | |
| 296.7 | $10^- \rightarrow 8^-$ | 886.8 | 1.12(17) | 22(1) | |
| 419.2 | $10^- \rightarrow 9^-$ | | 0.68(8) | 2(1) | 4 |
| 358.4 | $12^- \rightarrow 10^-$ | 1245.3 | 1.02(15) | 45(2) | |
| 502.0 | $12^- \rightarrow 11^-$ | | 0.58(6) | 6(1) | 4 |
| 424.4 | $14^- \rightarrow 12^-$ | 1669.7 | 1.03(10) | 68(4) | |
| 567.2 | $14^- \rightarrow 13^-$ | | 0.64(8) | 7(1) | 4 |
| 491.6 | $16^- \rightarrow 14^-$ | 2161.3 | 0.95(10) | 75(5) | |
| (620.0) | $16^- \rightarrow 15^-$ | | 0.59(7) | 8(1) | 4 |
| 581.9 | $(17^-) \rightarrow 16^-$ | 2314.9 | | 33(7) | 4 |
| 554.9 | $18^- \rightarrow 16^-$ | 2716.2 | 1.12(7) | 81(6) | |
| 634.4 | $(19^-) \rightarrow (17^-)$ | 2949.4 | | 22(4) | |
| 615.2 | $20^- \rightarrow 18^-$ | 3331.4 | 0.94(9) | 72(6) | |
| 693.9 | $(21^-) \rightarrow (19^-)$ | 3643.3 | | 22(4) | |
| 666.0 | $22^- \rightarrow 20^-$ | 3997.4 | 1.02(10) | 57(4) | |
| 754.3 | $(23^-) \rightarrow (21^-)$ | 4397.6 | 0.94(14) | 20(4) | |
| 710.8 | $24^- \rightarrow 22^-$ | 4708.2 | 0.97(15) | 49(4) | |
| 799.3 | $(25^-) \rightarrow (23^-)$ | 5196.9 | 0.89(18) | 19(4) | |
| 758.2 | $26^- \rightarrow 24^-$ | 5466.4 | 1.03(15) | 40(3) | |
| 837.2 | $(27^-) \rightarrow (25^-)$ | 6034.1 | 1.05(21) | 13(3) | |
| 808.7 | $28^- \rightarrow 26^-$ | 6275.1 | 1.04(16) | 21(1) | |
| 886.2 | $(29^-) \rightarrow (27^-)$ | 6920.3 | | 9(2) | |
| 862.8 | $30^- \rightarrow 28^-$ | 7137.9 | 0.86(17) | 14(1) | |
| 938.8 | $(31^-) \rightarrow (29^-)$ | 7859.1 | 0.92(18) | 7(1) | |
| 910.6 | $32^- \rightarrow 30^-$ | 8048.5 | 1.05(21) | 9(1) | |
| 994.4 | $(33^-) \rightarrow (31^-)$ | 8853.5 | | $\leqslant 3$ | |
| 953.0 | $(34^-) \rightarrow 32^-$ | 9001.5 | | $\leqslant 3$ | |
| **Band 6** | | | | | |
| | $(6^+)$ | x | | | |
| 94.8 | $(7^+) \rightarrow (6^+)$ | x+94.8 | 0.55(10) | 11(3) | |

TABLE I. (*Continued.*)

| $E_\gamma$[a] | $I_i^\pi \to I_f^\pi$[b] | $E_i$ | DCO | $I_\gamma$ | N |
|---|---|---|---|---|---|
| 220.8 | $(8^+) \to (6^+)$ | x+220.8 | | $\leqslant 3$ | |
| 126.0 | $(8^+) \to (7^+)$ | | 0.68(16) | 38(5) | |
| 279.3 | $(9^+) \to (7^+)$ | x+374.1 | 0.87(13) | 74(12) | |
| 153.3 | $(9^+) \to (8^+)$ | | 0.71(11) | 76(19) | |
| 326.4 | $(10^+) \to (8^+)$ | x+547.3 | 0.92(9) | 64(5) | |
| 173.2 | $(10^+) \to (9^+)$ | | 0.65(7) | 58(16) | |
| 377.5 | $(11^+) \to (9^+)$ | x+751.6 | 0.96(10) | 90(13) | |
| 204.3 | $(11^+) \to (10^+)$ | | 0.67(7) | 81(13) | |
| 409.7 | $(12^+) \to (10^+)$ | x+956.4 | 0.96(10) | 201(13) | |
| 204.8 | $(12^+) \to (11^+)$ | | 0.67(10) | 67(6) | |
| 460.4 | $(13^+) \to (11^+)$ | x+1212.1 | 0.87(11) | 101(10) | |
| 255.7 | $(13^+) \to (12^+)$ | | 0.76(8) | 39(7) | |
| 477.1 | $(14^+) \to (12^+)$ | x+1433.5 | 0.92(4) | 226(13) | |
| 221.4 | $(14^+) \to (13^+)$ | | 0.70(11) | 27(6) | |
| 527.3 | $(15^+) \to (13^+)$ | x+1739.4 | 0.94(10) | 91(10) | |
| 305.9 | $(15^+) \to (14^+)$ | | 0.50(8) | 17(3) | |
| 534.8 | $(16^+) \to (14^+)$ | x+1968.3 | 0.89(4) | 191(6) | |
| 228.9 | $(16^+) \to (15^+)$ | | 0.53(11) | 18(1) | |
| 579.0 | $(17^+) \to (15^+)$ | x+2318.4 | 0.99(6) | 85(6) | |
| 580.9 | $(18^+) \to (16^+)$ | x+2549.2 | 1.06(6) | 128(12) | |
| 610.1 | $(19^+) \to (17^+)$ | x+2928.6 | 0.90(9) | 35(7) | |
| 620.4 | $(20^+) \to (18^+)$ | x+3169.6 | 0.83(8) | 121(10) | |
| 648.0 | $(21^+) \to (19^+)$ | x+3576.6 | 0.99(10) | 24(6) | |
| 663.4 | $(22^+) \to (20^+)$ | x+3833.0 | 0.85(9) | 92(10) | |
| 693.8 | $(23^+) \to (21^+)$ | x+4270.3 | 1.02(10) | 18(4) | |
| 717.2 | $(24^+) \to (22^+)$ | x+4550.2 | 1.01(10) | 58(6) | |
| 750.5 | $(25^+) \to (23^+)$ | x+5020.9 | 0.92(9) | 16(4) | |
| 780.2 | $(26^+) \to (24^+)$ | x+5330.4 | 0.90(14) | 39(4) | |
| 814.1 | $(27^+) \to (25^+)$ | x+5834.9 | 0.99(12) | 12(3) | |
| 846.4 | $(28^+) \to (26^+)$ | x+6176.8 | 0.94(14) | 34(4) | |
| 880.3 | $(29^+) \to (27^+)$ | x+6715.3 | 0.91(14) | 10(2) | |
| 909.0 | $(30^+) \to (28^+)$ | x+7085.8 | 1.04(16) | 23(2) | |
| 938.5 | $(31^+) \to (29^+)$ | x+7653.8 | 1.03(15) | 8(3) | |
| 992.6 | $(32^+) \to (30^+)$ | x+8078.4 | 1.19(24) | 8(2) | |
| 1014.5 | $(33^+) \to (31^+)$ | x+8668.3 | 0.96(19) | 5(2) | |
| 1017.6 | $(34^+) \to (32^+)$ | x+9096.0 | | $\leqslant 3$ | |
| 1060.4 | $(35^+) \to (33^+)$ | x+9728.8 | | $\leqslant 3$ | |
| 1074.0 | $(36^+) \to (34^+)$ | x+10170.0 | | $\leqslant 3$ | |
| 1100.0 | $(37^+) \to (35^+)$ | x+10828.8 | | $\leqslant 3$ | |
| **Band 7** | | | | | |
| 938.0 | $(32^+) \to (30^+)$ | x+8023.8 | 0.94(4) | 13(2) | 6 |
| 931.8 | $(34^+) \to (32^+)$ | x+8955.6 | 1.02(20) | 7(1) | |
| 999.0 | $(36^+) \to (34^+)$ | x+9954.6 | 0.82(16) | 5(1) | |
| 1063.2 | $(38^+) \to (36^+)$ | x+11017.8 | 1.00(20) | 5(1) | |
| 1129.0 | $(40^+) \to (38^+)$ | x+12147.5 | | $\leqslant 3$ | |
| 1194.6 | $(42^+) \to (40^+)$ | x+13342.1 | | $\leqslant 3$ | |
| 1247.8 | $(44^+) \to (42^+)$ | x+14589.9 | | $\leqslant 3$ | |
| **Band 8** | | | | | |
| | $(8^+)$ | y | | | |
| 156.4 | $(9^+) \to (8^+)$ | y+156.5 | | $\leqslant 3$ | |
| 330.4 | $(10^+) \to (8^+)$ | y+330.0 | | $\leqslant 3$ | |
| 173.5 | $(10^+) \to (9^+)$ | | 0.66(3) | $\leqslant 3$ | |
| 378.0 | $(11^+) \to (9^+)$ | y+534.5 | | $\leqslant 3$ | |
| 204.4 | $(11^+) \to (10^+)$ | | 0.70(10) | $\leqslant 3$ | |
| 419.2 | $(12^+) \to (10^+)$ | y+750.0 | | $\leqslant 3$ | |
| 215.5 | $(12^+) \to (11^+)$ | | 0.74(15) | $\leqslant 3$ | |
| 467.5 | $(13^+) \to (11^+)$ | y+1002.0 | | $\leqslant 3$ | |

TABLE I. (*Continued.*)

| $E_\gamma$[a] | $I_i^\pi \to I_f^\pi$[b] | $E_i$ | DCO | $I_\gamma$ | N |
|---|---|---|---|---|---|
| 252.0 | $(13^+) \to (12^+)$ | | 0.74(15) | $\leqslant 3$ | |
| 517.2 | $(14^+) \to (12^+)$ | y+1267.0 | 1.02(20) | 21(10) | |
| 265.0 | $(14^+) \to (13^+)$ | | 0.59(12) | 18(9) | |
| 553.9 | $(15^+) \to (13^+)$ | y+1556.0 | 1.13(23) | 9(1) | |
| 289.0 | $(15^+) \to (14^+)$ | | 0.58(12) | 7(1) | |
| 585.1 | $(16^+) \to (14^+)$ | y+1852.0 | 1.34(20) | 26(9) | |
| 296.0 | $(16^+) \to (15^+)$ | | 0.74(15) | 19(7) | |
| 585.1 | $(17^+) \to (15^+)$ | y+2141.0 | 0.99(15) | 58(5) | |
| 289.0 | $(17^+) \to (16^+)$ | | 0.58(12) | 36(4) | |
| 589.8 | $(18^+) \to (16^+)$ | y+2441.8 | 1.35(20) | 50(18) | |
| 600.3 | $(19^+) \to (17^+)$ | y+2741.3 | 1.21(18) | 62(5) | |
| 625.3 | $(20^+) \to (18^+)$ | y+3067.1 | 1.09(16) | 36(2) | |
| 649.1 | $(21^+) \to (19^+)$ | y+3390.4 | 0.97(15) | 51(5) | |
| 679.9 | $(22^+) \to (20^+)$ | y+3747.0 | 1.03(15) | 30(3) | |
| 704.8 | $(23^+) \to (21^+)$ | y+4095.2 | 1.08(14) | 48(5) | |
| 734.9 | $(24^+) \to (22^+)$ | y+4481.9 | 0.98(14) | 20(2) | |
| 760.0 | $(25^+) \to (23^+)$ | y+4855.2 | 1.00(15) | 45(4) | |
| 789.7 | $(26^+) \to (24^+)$ | y+5270.5 | 1.09(15) | 14(2) | |
| 815.8 | $(27^+) \to (25^+)$ | y+5671.0 | 0.99(15) | 35(4) | |
| 844.7 | $(28^+) \to (26^+)$ | y+6115.2 | 1.03(21) | 9(1) | |
| 876.7 | $(29^+) \to (27^+)$ | y+6547.7 | 1.13(23) | 27(3) | |
| 906.1 | $(30^+) \to (28^+)$ | y+7021.3 | 0.93(19) | 6(1) | |
| 941.1 | $(31^+) \to (29^+)$ | y+7488.8 | 1.01(20) | 14(2) | |
| 971.2 | $(32^+) \to (30^+)$ | y+7992.5 | 0.93(19) | 5(1) | |
| 1006.2 | $(33^+) \to (31^+)$ | y+8495.8 | 0.91(18) | 11(2) | |
| 1030.1 | $(34^+) \to (32^+)$ | y+9022.6 | 1.03(21) | 5(1) | |
| 1045.0 | $(35^+) \to (33^+)$ | y+9541.4 | 1.13(23) | ≈7(2)[c] | |
| 1071.8 | $(36^+) \to (34^+)$ | y+10094.4 | 1.36(27) | 4(1) | |
| 1045.0 | $(37^+) \to (35^+)$ | y+10586.4 | | ≈6(2)[c] | |
| 1103.3 | $(38^+) \to (36^+)$ | y+11198.4 | 1.16(23) | $\leqslant 3$ | |
| 1072.6 | $(39^+) \to (37^+)$ | y+11659.0 | | $\leqslant 3$ | |
| 1145.8 | $(40^+) \to (38^+)$ | y+12339.4 | | $\leqslant 3$ | |
| 1183.9 | $(42^+) \to (40^+)$ | y+13523.3 | | $\leqslant 3$ | |

[a]Uncertainties in $\gamma$-ray energies are 0.2 keV for most transitions, except for relatively weak transitions (<10 units) where 0.5-keV uncertainties are appropriate.
[b]Less certain $I^\pi$ assignments are given in parentheses.
[c]Possible contamination due to unresolved multiplets.

ing transition from Band 2 to Band 3, 88 keV ($10^- \to 9^-$), has been observed as well. The *eA* signature has been extended up to spin 43 and *fA* signature to 50, which is the highest spin observed in the level scheme. The new high-spin transitions can be seen clearly in the coincidence spectra of Band 2 in Fig. 4. We note that the 610.4-, 648.6-, and 694.6-keV transitions placed above the $18^-$ state of the *fA* sequence in Ref. [24] are not confirmed by our data.

Extensive cross talk between Bands 2 and 4 was observed for the first time in the spin region of $17 \leqslant I \leqslant 27$. The mixing of the two bands indicates that they must have the same parity ($\pi = -$). The multipolarities of many interband transitions were deduced based on the measured DCO ratios. For example, the DCO ratios of 657-, 642-, and 568-keV $\gamma$ rays from Band 2 to Band 4 are all consistent with stretched $E2$ nature. The same is true for the 703-, 609-, and 600-keV $\gamma$ rays from Band 4 to Band 2. Likewise, the stretched $M1$

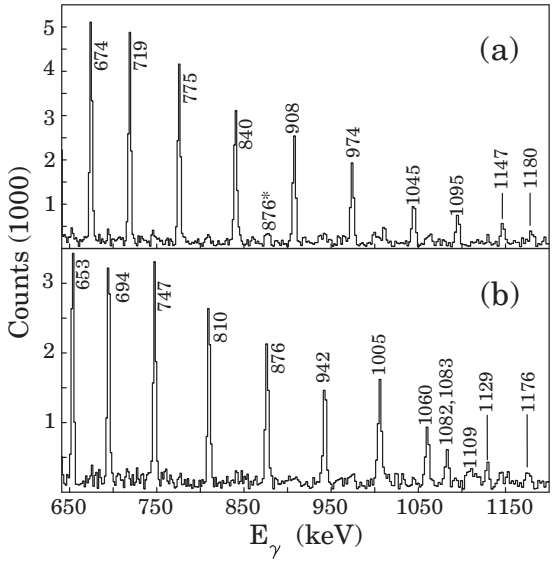


FIG. 3. Summed fourfold coincidence spectra for Band 1. (a) Spectrum for the $\alpha = 1$ signature, obtained by summing triple gates set on the transitions between $13^+$ and $41^+$. (b) Spectrum for the $\alpha = 0$ signature, obtained by summing triple gates set on the transitions between $16^+$ and $44^+$, but excluding 1005 keV. In all the following spectra coincidence $\gamma$ rays in other known bands are labeled with asterisks ($*$), and important interband linking transitions with plus ($+$) signs.

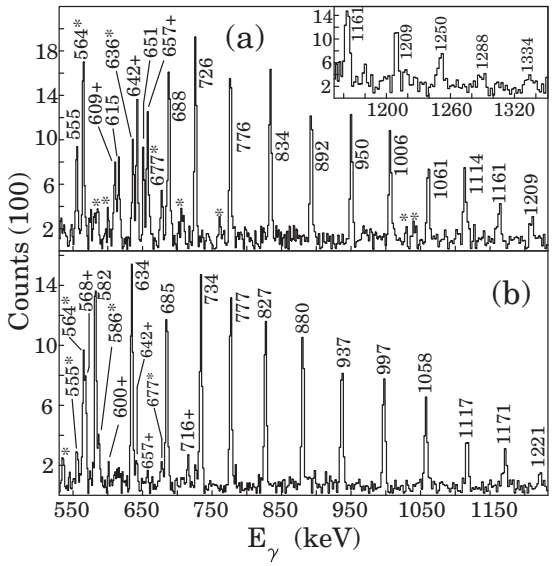


FIG. 4. Coincidence spectra for Band 2. Panel (a) shows summed fourfold coincidence spectra gated on transitions in the $\alpha = 0$ signature, between $14^-$ and $46^-$. The 609-, 642-, and 657-keV transitions linking Bands 2 and 4 can be seen clearly. The inset, which emphasizes the high-spin transitions, shows the sum of double gates set on transitions between $26^-$ and $50^-$. Panel (b) shows summed fourfold coincidence spectra gated on transitions in the $\alpha = 1$ signature, between $19^-$ and $41^-$. The 568-, 600-, 642-, 657-, and 716-keV transitions linking Bands 2 and 4 are visible.

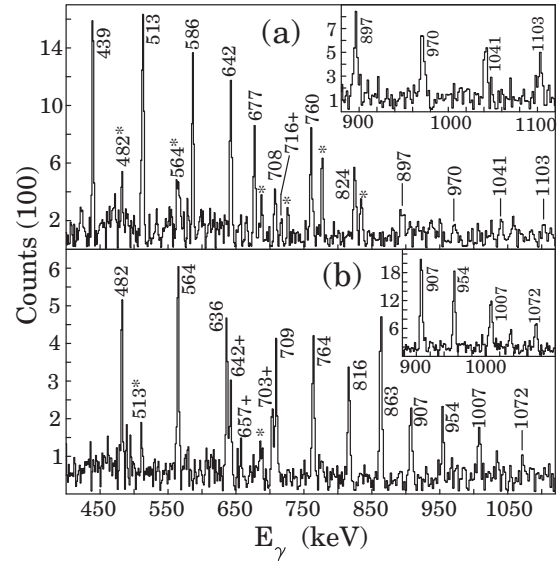


FIG. 5. Summed fourfold coincidence spectra for Band 4, with insets emphasizing the high-spin band members. (a) Spectrum for the $\alpha = 1$ signature, obtained by summing triple gates set on the transitions between $9^-$ and $37^-$, but excluding 760 and 824 keV. The 716-keV linking transition between this band and Band 2 is seen clearly. The inset is a sum of spectra double-gated on transitions between $27^-$ and $37^-$. (b) Spectrum for the $\alpha = 0$ signature, obtained by summing triple gates set on the transitions between $14^-$ and $34^-$ but excluding 863 keV. The 642-, 657-, and 703-keV linking transitions between this band and Band 2 are clearly visible. The peak at 1035 keV is a contamination. The inset is a sum of spectra double-gated on transitions between $22^-$ and $36^-$.

nature is confirmed for the 319-, 308-, and 324-keV $\gamma$ rays from Band 2 to Band 4, as well as the 343- and 316-keV $\gamma$ rays from Band 4 to Band 2. The level spins and energies in Band 4 could therefore be determined. Band 4 has been extended from spin 24 to (36) and from 21 to (37) for signatures *gB* and *gA*, respectively. The coincidence spectra showing the high-spin region of Band 4 are displayed in Fig. 5.

Band 5 is observed for the first time in the present work. The *hA* signature decays to Band 4 via parallel $\gamma$ rays with energies of 419.2, 502.0, 567.2 and, possibly, 620.0 keV. The respective DCO ratios, 0.68(8), 0.58(6), 0.64(8) and 0.59(7), are in agreement with stretched dipole character, indicating even spins for this sequence. The *hB* sequence feeds the $16^-$ state in Band 4 via a 581.9-keV $\gamma$ ray, which is the only depopulating transition observed. This sequence is the weakest in the level scheme, and no DCO ratio could be extracted for any of its transitions. The sequences *hA* and *hB* are suggested to be signature partners, and a negative parity is proposed for Band 5 based on its rotational properties. Detailed discussion will be presented in Sec. IV G. Fig. 6 shows the coincidence spectra of Band 5, where most linking transitions may be seen.

### B. Bands 6–8

Band 6 was observed in previous studies using different reactions, and was associated with a positive parity based on the proposed configurations [24,26]. Its intensity diminishes at

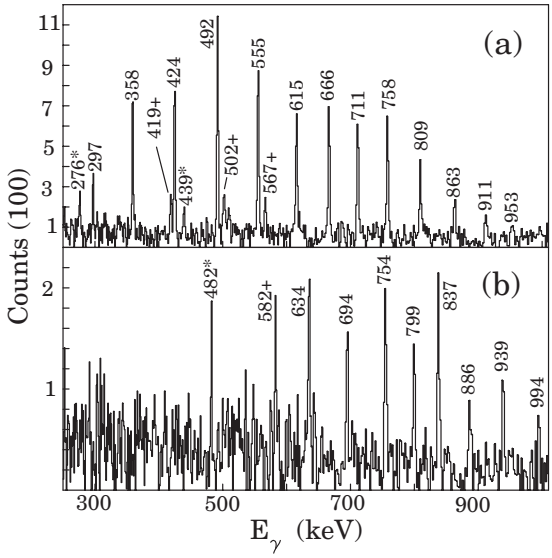


FIG. 6. Summed fourfold coincidence spectra for Band 5. (a) Spectrum for the $\alpha = 0$ signature, obtained by summing triple gates set on the transitions between $8^-$ and $34^-$. The 419-, 502- and 567-keV decays to Band 4 are clearly visible. (b) Spectrum for the $\alpha = 1$ signature, obtained by summing triple gates set on the transitions on the decay path from $(33^-)$ in Band 5 to $14^-$ in Band 4, but excluding 634 keV. The 582-keV decay to Band 4 is clearly visible.

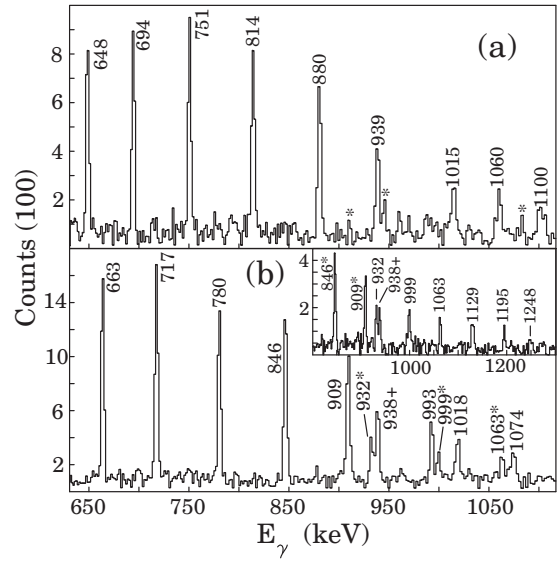


FIG. 7. Summed fourfold coincidence spectra for Bands 6 and 7. (a) Spectrum for the $\alpha = 1$ signature of Band 6, obtained by summing triple gates set on the transitions between $(17^+)$ and $(37^+)$. (b) Spectrum for the $\alpha = 0$ signature of band 6, obtained by summing triple gates set on the transitions between $(16^+)$ and $(36^+)$. The 938-keV transition linking this band to Band 7 is clearly visible. The inset shows the spectrum for Band 7 obtained by summing triple gates on all transitions on the decay path from $(44^+)$ in Band 7 and $(16^+)$ in Band 6.

low spins ($I < 15\ \hbar$), indicating a fragmented decay pathway. It feeds Band 1 at spin 13 and below, but linking transitions were not identified, and consequently level spins could not be firmly determined. The band, previously observed up to $I = (22)$, has been extended to a spin value of (37).

Band 7, observed to spin $(44^+)$, is reported here for the first time. It feeds the $(30^+)$ level of Band 6 via a 938-keV linking transition, whose DCO ratio of 0.94(4) is consistent with stretched E2 character. Thus, the band must have the same parity and signature with the *dA* sequence, i.e., positive parity and even signature. The coincidence spectra for Bands 6 and 7 are presented in Fig. 7.

Band 8 is also observed for the first time. Coincidence spectra for this band are presented in Fig. 8. It is assigned to $^{168}$Lu on the basis of evidence that it decays to Band 1 at spin 14 and below, i.e., the band is in coincidence with 448-, 408-, 363-, 314-, 258-, and 193-keV low-spin transitions in Band 1. Band 8 shows a loss of intensity below spin (18), suggesting that the decay out is from this level and below. However the decay pathways between the two bands could not be established. A positive parity is suggested for the band based on the proposed configurations, as discussed in Sec. IV H.

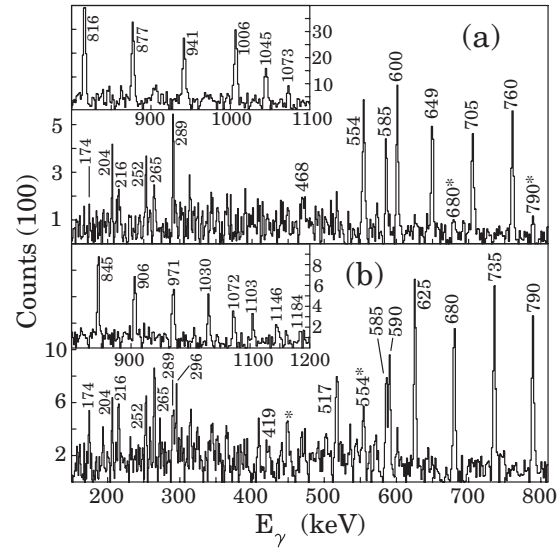


FIG. 8. Summed fourfold coincidence spectra for Band 8, with insets emphasizing high-spin band members. (a) Spectrum for the $\alpha = 1$ signature, obtained by summing triple gates set on the transitions between $(11^+)$ and $(39^+)$. The inset was obtained by summing double gates set on band members between $(17^+)$ and $(39^+)$, but excluding 760 and 1006 keV. (b) Spectrum for the $\alpha = 0$ signature, obtained by summing triple gates set on the transitions between $(10^+)$ and $(42^+)$. The inset was generated by summing double gates set on band members between $(40^+)$ and $(26^+)$.

## IV. DISCUSSION

### A. CSM calculations

To understand the intrinsic configurations and the underlying physics of the bands, we compared their observed dynamical properties with the predictions of CSM calculations. Theoretical quasiparticle Routhians were generated

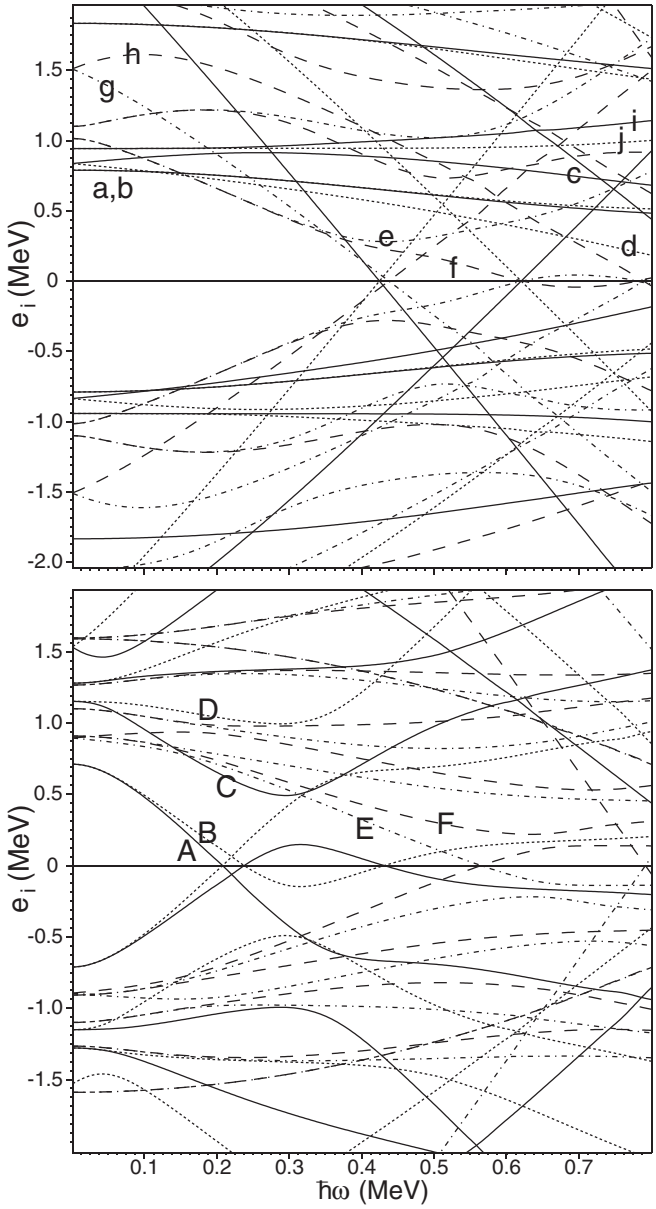


FIG. 9. Quasiparticle Routhians as a function of rotational frequency for protons (upper panel) and neutrons (lower panel), generated with the code ULTIMATE CRANKER [14,15] for $^{168}$Lu for an axially symmetric potential with a quadrupole deformation of $\epsilon = 0.25$. Solid lines denote quasiparticle levels with $(\pi, \alpha) = (+, +\frac{1}{2})$; dotted lines denote $(+, -\frac{1}{2})$; dash-dotted lines denote $(-, +\frac{1}{2})$ and dashed lines $(-, -\frac{1}{2})$. Upper case letters identify relevant neutron orbitals, and lower case letters proton orbitals. The labeling convention is explained in Table II.

using the UC code [14,15], and are shown in Fig. 9. The labeling of the quasiparticles and related orbitals closest to the Fermi surface are listed in Table II, where each letter corresponds to a state described by a given combination of asymptotic Nilsson orbitals and by appropriate signature ($\alpha$) and parity quantum numbers. Calculated alignments of each orbital are also shown in the table.

TABLE II. Labels and alignments ($i_x$) of theoretical Routhians for $^{168}$Lu. Lower case letters denote protons, and upper case letters neutrons. The spherical shell model (SSM) states represent only the main components of the wave functions, if the orbitals are mixed. The up (↑) and down (↓) arrows indicate whether the spin and orbital angular momenta are parallel ("spin up") or antiparallel ("spin down"), respectively.

| SSM states | Nilsson orbital | $\alpha = +1/2$ | $i_{x,\alpha=+}$ | $\alpha = -1/2$ | $i_{x,\alpha=-}$ |
|---|---|---|---|---|---|
| $\pi g_{7/2}$ | $[404]7/2^+ \downarrow$ | a | 0.4 | b | 0.4 |
| $\pi d_{3/2}$ | $[411]1/2^+ \downarrow$ | c | 0 | d | 0.5 |
| $\pi d_{5/2}$ | $[402]5/2^+ \uparrow$ | i | −0.1 | j | 0 |
| $\pi h_{11/2}$ | $[514]9/2^- \uparrow$ | e | 2.0 | f | 2.0 |
| $\pi h_{9/2}$ | $[541]1/2^- \downarrow$ | g | 3.5 | h | 1.6 |
| $\nu i_{13/2}$ | $[642]5/2^+ \uparrow$ | A | 4.1 | B | 3.3 |
| $\nu i_{13/2}$ | $[651]3/2^+ \uparrow$ | C | 3.1 | D | 0.7 |
| $\nu h_{9/2}$ | $[523]5/2^- \downarrow$ | E | 3 | F | 1.3 |

It was thus possible to compare the measured aligned angular momenta (alignments) and possible crossings of band structures with the theoretical values. Further interpretative constraints are provided by the excitation energies and energy splitting between signature partners. A systematic investigation of all the observed bands was carried out with respect to these observables, and compared with the single proton and neutron orbitals observed in the neighboring nuclei. The single proton orbitals observed are $[404]7/2^+$, $[411]1/2^+$, $[402]5/2^+$, $[514]9/2^-$, $[541]1/2^-$ in $^{167}$Lu [20] and $^{169}$Lu [29]. The lowest single neutron orbitals observed are $[642]5/2^+$, $[651]3/2^+$, $[523]5/2^-$ in $^{167}$Yb [30] and $^{169}$Hf [31].

In Fig. 10 the experimental alignments of all the bands are displayed as a function of rotational frequency. It should be pointed out that the spins and excitation energies of Bands 6, 7, and 8 are uncertain since they are not connected to other known states in the level scheme. But the rotational frequency is nearly independent in a range of a few $\hbar$ of possible spin assignment. Fig. 11 provides the measured excitation energies of Bands 1, 2, 4, and 5 relative to a rigid-rotor reference $AI(I+1)$, where the inertia parameter $A$ was chosen to be 7.4 keV. It may be seen in Fig. 11 that the $fA$ sequence of Band 2 is yrast at spin 22 and above, the positive-parity Band 1 becomes yrast at spin 14 and below, and the $gB$ sequence of Band 4 is yrast between spins $16-20$. This makes $gB$ the strongest negative-parity sequence in the low-spin regime. A summary of the assigned configurations and features of the band crossings is given in Table III. The band crossing frequencies were extracted using the dynamical moments of inertia plots in Fig. 12 and the alignment plots in Fig. 10.

### B. $B(M1)/B(E2)$ ratios

For strongly coupled bands with $\Delta I$=1 mixed $M1/E2$ connecting transitions, the experimental values of $B(M1)/B(E2)$

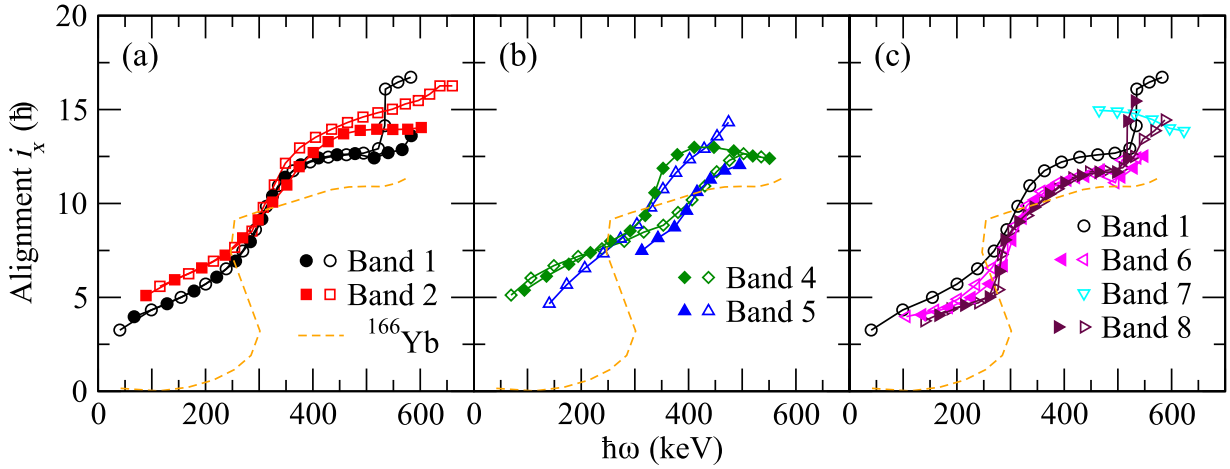


FIG. 10. Aligned angular momenta of bands in $^{168}$Lu. The curve for the yrast band of the even-even $^{166}$Yb has been superimposed on each panel as a reference. Open symbols represent $\alpha = 0$ sequences and closed symbols $\alpha = 1$ sequences. A reference with Harris parameters $J_0 = 30\ \hbar^2\text{MeV}^{-1}$ and $J_1 = 45\ \hbar^4\text{MeV}^{-3}$ was subtracted from the data.

ratios were extracted using the standard expression

$$\frac{B(M1, I \to I-1)}{B(E2, I \to I-2)} = 0.697\left(\frac{T_1}{T_2}\right)\left(\frac{E_2^5}{E_1^3}\right)\left(\frac{1}{1+\delta^2}\right),$$

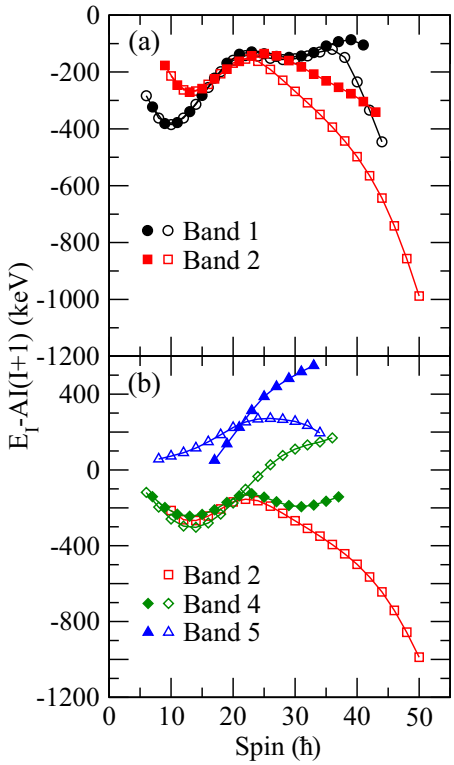


FIG. 11. Excitation energies less a rigid rotor reference ($A = 7.4$ keV) as a function of spin. Open symbols represent $\alpha = 0$ and filled symbols $\alpha = 1$ sequences. The $\alpha = 0$ signature of Band 2 has been duplicated in the lower panel to provide a reference.

where the branching ratio is

$$\lambda = \frac{T_2}{T_1} = \frac{T_\gamma(\Delta I = 2)}{T_\gamma(\Delta I = 1)},$$

and $T_\gamma(\Delta I = 2)$ and $T_\gamma(\Delta I = 1)$ are the respective $\gamma$-ray intensities of the $\Delta I = 2$ and $\Delta I = 1$ transitions. The influence of the mixing ratio $\delta^2 = T_1(E2)/T_1(M1)$ can be estimated from the results of rigid-rotor calculations [1]. The correction is in general less than 10% and has therefore been neglected, with the result that the "experimental" values should be understood as upper limits of the actual ones. The ratios are

TABLE III. A summary of the quasiparticle configurations proposed, and the band crossing frequencies, $\hbar\omega_c$, observed in $^{168}$Lu.

| Band | Configurations | $\hbar\omega_c$ |
|---|---|---|
| 1 | $aA \to aABC$ | 0.31 |
| | $bA \to bABC$ | 0.31 |
| | $aABC \to aABCfg$ | >0.54 |
| | $bABC \to bABCfg$ | 0.54 |
| 2 | $eA \to eABC$ | 0.32 |
| | $fA \to fABC$ | 0.32 |
| | $fABC \to fABCEF$ | ≈0.63 |
| 3 | $aE$ | |
| | $bE$ | |
| 4 | $gA \to gABC$ | 0.34 |
| | $gB \to gBAD$ | 0.44 |
| 5 | $hA \to hABC$ | 0.35 |
| | $hB \to hBAD$ | 0.45 |
| 6 | $cA \to cABC$ | 0.30 |
| | $dA \to dABC$ | 0.30 |
| | $cABC \to cABCfg$ | >0.54 |
| | $dABC \to dABCfg$ | >0.53 |
| 7 | $fABCDE$ | |
| 8 | $iA \to iABC$ | 0.28 |
| | $jA \to jABC$ | 0.28 |
| | $iABC \to iABCfg$ | 0.53 |
| | $jABC \to jABCfg$ | >0.54 |

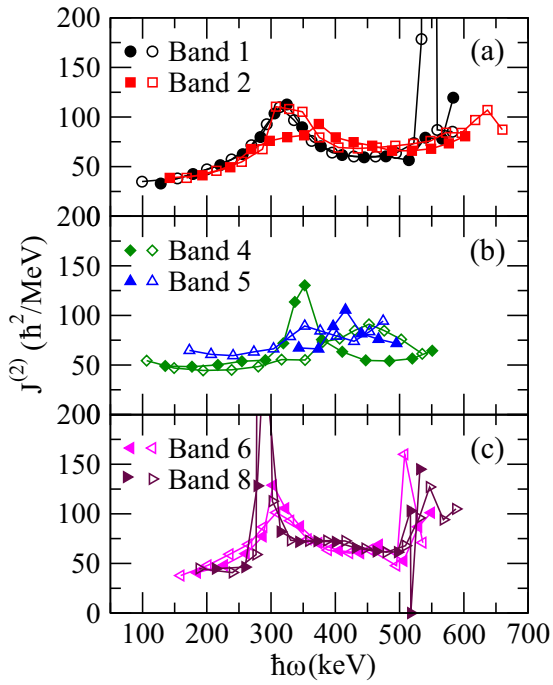


FIG. 12. Dynamical moments of inertia, $J^{(2)}$, for bands in $^{168}$Lu. Open (filled) symbols represent $\alpha = 0$ ($\alpha = 1$) sequences.

compared in Fig. 13 with theoretical estimates which are based on an extension of Dönau's geometric model [32]

$$B(M1, I \to I-1) = \frac{3\mu_N^2}{8\pi I^2}\left\{\sqrt{I^2-K^2}\left[\sum_j (g_j - g_R)\Omega_j\right] - K\left[\sum_j (g_j - g_R) i_j\right]\right\}^2$$

and the rotational form of the $B(E2)$ strength

$$B(E2, I \to I-2) = \frac{5}{16\pi} Q_0^2 \langle I_i K 20 | I_f K\rangle^2.$$

The collective gyromagnetic ratio of the core ($g_R$) was taken to be $Z/A = 0.42$ in the calculation. The intrinsic quadrupole moment $Q_0 = 6.8$ eb was adopted from the UC calculation, with a 15% larger value used for Band 4 where the strongly deformation-driving $\pi[541]1/2^-$ orbital is involved [20]. The intrinsic $g$-factors ($g_j$) used for different quasiparticle orbitals were taken from Refs. [31,33], where they had been calculated from the wave functions in Ref. [34]. The aligned angular momenta for the odd proton and odd neutron ($i_j$) were extracted from $^{167}$Lu [20] and $^{169}$Hf [31], respectively. The parameter values for neutrons are $g_n = -0.3$, $\Omega_n = 2.5$, and $i_n = 4.1$ for all bands in the calculation. For protons, the parameters are listed in Table IV together with the $K$ values extracted for each band, as will be described shortly.

Measured $B(M1)/B(E2)$ ratios are strongly dependent on the active quasiparticles. As discussed below, each of the two-quasiparticle bands in $^{168}$Lu involves a different quasiproton coupled with the same neutron $[642]5/2^+$ orbital (except for Band 3). Consequently, the $B(M1)/B(E2)$ ratios can be

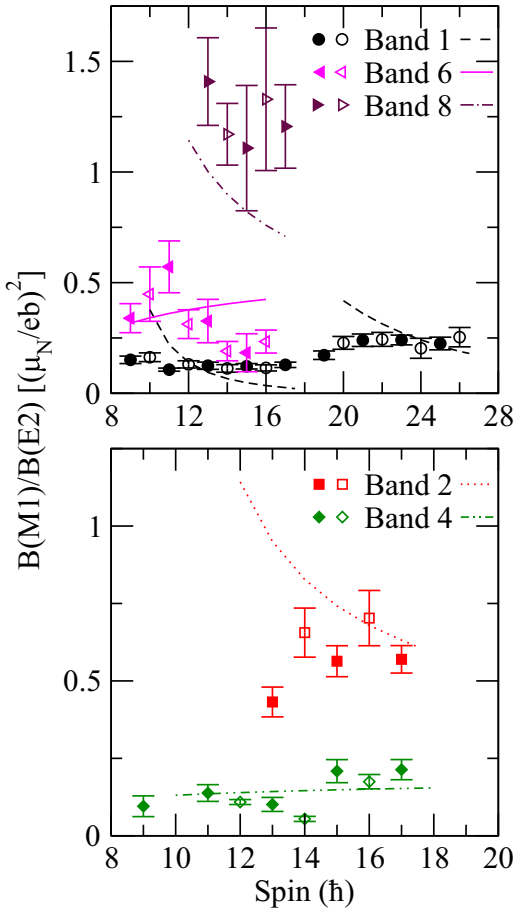


FIG. 13. Experimental (data points) and theoretical (lines) $B(M1)/B(E2)$ ratios for bands in $^{168}$Lu. The values for positive- and negative-parity bands are plotted in the upper and lower panels, respectively. Open (filled) symbols represent the experimental values for the $\alpha = 0$ ($\alpha = 1$) sequences. The spins of Bands 6 and 8 are uncertain. See text for discussion.

a sensitive probe of the active quasiproton in a band. The experimental and theoretical $B(M1)/B(E2)$ ratios agree fairly well for all bands calculated, which provided strong support for the proposed band configurations.

### C. Band 1 (*aA*, *bA*)

Band 1 undergoes a crossing at $\hbar\omega \approx 0.31$ MeV, with an associated alignment gain of $\Delta i_x \approx 8\,\hbar$ (Fig. 10). The alignment is consistent with the neutron *BC* crossing predicted by CSM calculations, as well as the *BC* crossings observed in neighboring nuclei, such as $^{167}$Yb [30], $^{169}$Hf [31], and

TABLE IV. Parameters used for calculation of $B(M1)/B(E2)$ ratios.

| | Band 1 | Band 2 | Band 4 | Band 6 | Band 8 |
|---|---|---|---|---|---|
| $g_p$ | 0.8 | 1.29 | 0.76 | −1.57 | 1.90 |
| $\Omega_p$ | 3.5 | 4.5 | 0.5 | 0.5 | 2.5 |
| $i_p$ | 0.4 | 1.8 | 3.5 | 0.0 | −0.1 |
| $K$ | 6.0 | 7.0 | 2.0 | 2.0 | 5.0 |

$^{167}$Lu [20]. The neutron *AB* crossing, as displayed for $^{166}$Yb in Fig. 10, is clearly missing. This fact indicates that the band configuration already contains the neutron orbital *A* and thus the *AB* crossing is blocked. The two signatures of Band 1 are therefore assigned configurations *aA* and *bA*. The measured initial aligned angular momenta ($\approx$4 $\hbar$) are close to the calculated values. We therefore concur with the suggested configuration of $\pi g_{7/2} \otimes \nu i_{13/2}$ for the band in previous publications [24,25]. This is further supported by the extracted $B(M1)/B(E2)$ values in Fig. 13.

There are two ways for the valence quasiproton and quasineutron to couple: with intrinsic spins parallel or antiparallel. According to the Gallagher-Moszkowski (G-M) rules [35], at the bandhead in well-deformed nuclei, the parallel coupling is generally energetically lower than the antiparallel one, with a splitting of 50 to 200 keV. The parallel coupling corresponds to $K = 1$, and the antiparallel coupling to $K = 6$. Although the G-M rules therefore suggest that $K = 1$ should be favored for Band 1, the high-*K* coupling was found to be $\approx$400 keV lower in energy than the low-*K* coupling of the $\pi g_{7/2} \otimes \nu i_{13/2}$ band throughout the odd-odd nuclei in this region, e.g., in $^{164}$Tm [36], $^{166}$Tm [37], and $^{170}$Ta [38]. The observed lowest level in Band 1 is $6^+$ at 27.2 keV above the $6^-$ ground state ($K = 6$). The 91.6 keV $E1$ transition decays from the $7^+$ state directly to the $6^-$ ground state, which would likely be hindered if Band 1 had $K = 1$ and $\bigtriangleup K = 6 - 1 = 5$ between Bands 1 and 3. This fact suggests that Band 1 has *K* value of 6, rather than 1, and that the $6^+$ level is the bandhead. Furthermore, it was found that the high-*K* coupling of Band 1 had a better agreement with the predicted additivity of Routhians (see Sec. IV J) than the low-*K* assignment. Therefore the band has a *K* value of 6.

The *bABC* sequence then exhibits a sharp up-bend at rotational frequency $\hbar\omega \approx 0.52$ MeV with an alignment gain $\geqslant$ 4.2$\hbar$. In this frequency range the most likely crossing is caused by proton alignment. The *ef* crossing is predicted around $\hbar\omega \approx 0.48$ MeV, associated with a small gain of $\Delta i \leqslant 2\hbar$ and a strong interaction ($\approx$250 keV) causing the alignment to be very gradual. The "hybrid" *fg* crossing is predicted to follow closely with $\approx$5 $\hbar$ alignment gain. The *fg* crossing comes with a weak interaction ($\approx$150 keV). One therefore expects a rather sharp up-bend to be associated with the *fg* crossing. The *fg* crossing seems to be a more likely explanation for the up-bend in *bABC* sequence. Indeed, the *fg* crossing has been identified in several neighboring nuclei, e.g., $^{167}$Lu [20], $^{167,168}$Yb [30], $^{168}$Hf [23], and $^{169}$Hf [31] in this frequency range. The onset of the crossing in signature *aA* at frequency $\approx$0.55 MeV is likely caused by the same proton crossing.

### D. Band 2 (*eA*, *fA*)

Like the previous band, Band 2 also undergoes a *BC* crossing around $\hbar\omega \approx 0.32$ MeV. Its initial alignment is 1.2 $\hbar$ greater than that of Band 1. At rotational frequencies above $\hbar\omega \approx 0.34$ MeV Band 2 undergoes pronounced splitting, consistent with the big splitting between the orbitals *e* and *f* in CSM calculations (Fig. 9). The configurations *eA* and *fA* can thus be assigned to the two signatures of Band 2 ($K^\pi = 7^-$), which agrees with the previously suggested configuration $\pi h_{11/2} \otimes \nu i_{13/2}$ for the band [24,25]. The measured $B(M1)/B(E2)$ ratios for the band (see Fig. 13) are consistent with predicted values that are much larger than those of Band 1. The low-spin $E1$ transitions from Band 2 to Band 1 are very similar to those observed in $^{169}$Lu from the $\pi[514]9/2^-$ band to $\pi[404]7/2^+$ band, where the $B(E1)$ transition probabilities were analyzed by invoking the octupole degree of freedom [29].

At higher spins, the alignments of the sequences *eABC*/*fABC* are higher (>1.5 $\hbar$) than those of the *aABC*/*bABC* sequences of Band 1 [see Fig 10(a)], which is caused by the larger initial alignments of the *e* and *f* orbitals as compared to orbitals *a* and *b*. No additional alignment gain is seen for the *eABC* sequence. However, the *fABC* sequence shows a gradual gain of 1.3 $\hbar$ between frequencies 0.43–0.6 MeV. The behavior of Band 2 is similar to that of the band built on $\pi[514]9/2^-$ orbital in $^{167}$Lu [20]. UC calculations predict that, above $\approx$0.4 MeV, a large signature splitting between the *e* and *f* proton orbitals is anticipated (see Fig. 9), resulting in different alignments for the *eABC* and *fABC* sequences. The excitation energies [see Fig. 11(a)] also show such a splitting, which makes the *fABC* sequence energetically very favorable. As a result, the sequence was observed to the highest spin in the level scheme.

The gradual gain of aligned angular momentum near the highest spins in the *fABC* sequence is also related to another crossing, as indicated by a broad bump in the plot of its dynamical moment of inertia (see Fig. 12), centered around $\hbar\omega \approx 0.63$ MeV. This crossing probably has a neutron origin, since both the proton *fg* and *ef* crossings are blocked. Since the neutron *CD* crossing is also expected to be blocked after the *BC* crossing, the remaining possibility is the *EF* crossing on the basis of UC calculations. Further support for this suggestion is that an *EF* crossing at a similar frequency was reported for the $\pi[514]9/2^-$ band in neighboring $^{167}$Lu [20] and $^{165}$Lu [39]. We therefore suggest that the *fABC* sequence undergoes an *EF* crossing, and ends up with a six-quasiparticle configuration, *fABCEF*.

The *eABC* signature is observed above the rotational frequency $\hbar\omega \approx 0.6$ MeV, which is beyond the proton *fg* crossing frequencies 0.52–0.55 MeV in Band 1, and also that in the band built on the signature *e* of the $\pi[514]9/2^-$ orbital in $^{167}$Lu [20]. Unlike the proton *ef* crossing, the *fg* crossing is not expected to be blocked in the *eABC* sequence. This raises the question: why is the *fg* crossing missing in this sequence? A possible explanation may be provided by band mixing. There is extensive cross talk between Bands 2 and 4 in the medium-spin region. Some levels in the two bands are nearly degenerate. For example, the energy differences between the respective $20^-$ and $25^-$ states in the two bands are as small as 6.0 and 8.2 keV. Clearly, the wave functions of Bands 2 and 4 are strongly mixed, which would make an *fg* crossing in the *eABC* sequence impossible since Band 4 is based on proton orbital *g*.

### E. Band 3 (*aE*, *bE*)

The $6^-$ ground state with a half-life of 5.5 min was identified from electron-capture decay experiments, and suggested

to have a configuration of $\pi[404]7/2^+ \otimes \nu[523]5/2^-$ [27,28]. Zhao *et al.* identified Band 3 and linked it with Bands 1 and 2 [26]. The negative parity of the band was deduced from the existence of the 343-keV ($9^- \rightarrow 7^-$) stretched $E2$ transition between Bands 2 and 3, which indicates that the bands have the same parity. The experimental $K$ quantum number and the rotational parameter of Band 3 were extracted by fitting its levels and comparing the values with those predicted from the neighboring odd-A nuclei. It was concluded that the values are consistent with those of the configuration $\pi[404]7/2^+ \otimes \nu[523]5/2^-$ with $K = 6$. This is identical to the ground state configuration, and Band 3 is therefore the ground state band. The present work confirms Band 3 and also its connections with Bands 1 and 2. We also agree with the proposed configuration for the band. The observed bandhead energy of 27 keV for Band 1 is very close to the predicted value of 34 keV, based on quasiparticle excitations in odd-mass nuclei adjacent to $^{168}$Lu [28]. While signatures $a$ and $b$ for $\pi[404]7/2^+$ orbital are degenerate, there is considerable splitting between signatures $E$ and $F$ for the $\nu[523]5/2^-$ orbital, as indicated by UC calculations and observed from the odd-$N$ neighbor $^{167}$Yb [30]. Experimentally, no splitting is seen between the two signatures of Band 3. Therefore configurations $aE$ and $bE$, rather than $aE$ and $aF$, are suggested for the band.

### F. Band 4 ($gA$, $gB$)

The $\alpha = 1$ signature ($gA$) undergoes a crossing at $\hbar\omega = 0.34$ MeV with $\approx 6\hbar$ alignment gain, which can be identified as a $BC$ crossing, as suggested in previous publications. The crossing occurs at a higher frequency than $BC$ crossings in the other bands. In this mass region delayed $\nu i_{13/2}$ band crossings are systematically observed in bands associated with the $\pi[541]1/2^-$ orbital. They are understood to be associated with increased deformation caused by the down-sloping deformation-driving proton $g$ orbital [40], together with a residual $pn$ interaction [36].

The $\alpha = 0$ sequence of Band 4 could be the neutron signature partner $gB$ or proton partner $hA$. However, the $hA$ configuration is expected to exhibit a $BC$ crossing. The sequence exhibits an alignment substantially beyond the $AB$ and $BC$ crossing frequencies, namely at $\hbar\omega \approx 0.44$ MeV, with a gain of only $\approx 4.4\hbar$. We ascribe this alignment to the calculated next available neutron crossing, $AD$, where both $AB$ and $BC$ crossings are blocked. This implies that the configuration must involve the neutron orbital $B$, and that the sequence has the configuration $gB$. Indeed, the $AD$ crossing has been reported in several neighboring nuclei where bands involve the neutron $B$ orbital, such as in $^{167}$Yb [30], $^{167}$Hf [41,42], $^{169}$Hf [31], and the even-even $^{168}$Hf [23]. Furthermore, the energy difference between the lower-spin states of the two signatures in Band 4, as seen in Fig. 11, is more in line with that between orbitals $A$ and $B$, and substantially smaller than that between orbitals $g$ and $h$ (see Fig. 9). This provides additional support that Band 4 consists of signatures $gA$ and $gB$ ($K^\pi = 2^-$), rather than $gA$ and $hA$. As presented in Fig. 13, the theoretical $B(M1)/B(E2)$ values of $gA/gB$ configuration for Band 4 and the experimental ratios are in good agreement.

In contrast to Band 1 and other positive-parity bands (Bands 6 and 8), Band 4 undergoes no further alignment beyond the neutron $BC$ and $AD$ crossings, at least certainly not below the highest measured frequency of $\approx 0.55$ MeV. This is consistent with the proposed configuration, where the proton $fg$ crossing is blocked in both signature partners. The $ef$ crossing and other neutron crossings are probably delayed on account of the larger deformation.

### G. Band 5 ($hA$, $hB$)

Band 5, observed for the first time, feeds the negative-parity Band 4 ($gA$, $gB$). Both bands exhibit similar rotational properties. For example, the $\alpha = 0$ ($hA$) sequence of Band 5 undergoes a crossing at $\hbar\omega \approx 0.35$ MeV with an alignment gain of $\Delta i_x > 5\hbar$, similar to the crossing present in the $gA$ sequence of Band 4, although $hA$ has a smaller initial alignment. This is identified as the $BC$ crossing. The remaining $\alpha = 1$ sequence ($hB$) undergoes a crossing at $\hbar\omega \approx 0.45$ MeV with a gain of $\Delta i_x > 4\hbar$, which is the analogue of the $AD$ crossing identified in the $gB$ sequence of Band 4. The lower-spin members of $\alpha = 1$ sequence could not be observed due to diminishing intensity near the bottom of band. The most probable scenario is that both sequences of Band 5 involve the unfavored signature $h$ of the $[541]1/2^-$ proton orbital, and that their configurations are $hA$ ($\alpha = 0$) and $hB$ ($\alpha = 1$), with $K^\pi = 3^-$.

Further support for the proposed configurations comes from the measured excitation energies of the bands. As seen in Fig. 11(b), sequence $hA$ lies about 400 keV above $gA$, and sequence $hB$ lies above $gB$ by a similar amount. This energy difference agrees with calculated large splitting between signatures $h$ and $g$ of the $\pi[541]1/2^-$ orbital shown in Fig. 9. The rather unique alignment pattern and the exceptionally high excitation energy are clear indications of the proposed configuration for the band, which also implies that Band 5 must have negative parity. Bands built on the unfavored signature of the proton $[541]1/2^-$ orbital have also been reported in this mass region, e.g., in $^{167}$Lu [20] and $^{165}$Tm [40].

### H. Bands 6 ($cA$, $dA$) and 8 ($iA$, $jA$)

Bands 6 and 8 undergo crossings at frequencies $\approx 0.3$ and $\approx 0.28$ MeV, respectively, with similar alignment gain of $\approx 5.5\hbar$; see Fig. 10(c). The alignment patterns are very similar to that of Band 1, and can also be identified as the $BC$ crossing. Consequently, both bands must involve the neutron orbital $A$. We next consider candidates for the active protons.

Whereas previous work associated Band 6 with the $\pi[402]5/2^+$ orbital [24], we reconsidered this configuration assignment. UC calculations indicate that both the $\pi[411]1/2^+$ and $\pi[402]5/2^+$ orbitals are close to the Fermi surface and that the former is actually lower in excitation energy (see Fig. 9). The $(i, j)$ Routhians of the $\pi[402]5/2^+$ orbital are nearly degenerate, but a moderate splitting exists between $(c, d)$ for $\pi[411]1/2^+$. Furthermore, of the four Routhians $d$ has the largest downslope, which is expected to generate a larger alignment. These properties are consistent with experimental observations in $^{167}$Lu [20] and $^{169}$Lu [29].

In our data, the signature splitting in Band 6 is substantially larger than that of Band 8 (see Sec. IV K). The alignment plot (Fig. 10(c)) also shows that the two signatures of Band 8 ($iA$ and $jA$) are degenerate. Before the $BC$ crossing, they have smaller alignments than the $\alpha = 1$ ($cA$) sequence of Band 6, while $\alpha = 0$ signature ($dA$) has an even larger alignment. Thus, Band 6 is likely associated with the $\pi[411]1/2^+$ orbital and Band 8 with $\pi[402]5/2^+$, which has higher excitation energy. Indeed, Band 8 is more weakly populated than Band 6. The suggested configurations are further supported by measured $B(M1)/B(E2)$ ratios in Fig. 13. The experimental ratios for Band 8 are substantially higher than those of Band 6, consistent with calculated ones. The uncertainties of the spin values in the two bands may cause small horizontal displacements of the measured data points together with theoretical curves, but do not move them vertically.

Another proton orbital near Fermi surface is the negative-parity $\pi[523]7/2^-$, which is calculated about 300 keV higher than the $\pi[402]5/2^+$ orbital at $\hbar\omega \leqslant 0.3$ MeV, and exhibits significant splitting above this frequency. Bands associated with this orbital have been observed in $^{164}$Tm [36] and $^{164}$Lu [43]. Their properties are substantially different than those of Bands 6 and 8, and so the $\pi[523]7/2^-$ orbital can be ruled out. We have therefore assigned the configuration $cA$ and $dA$ ($K^\pi = 2^+$) to Band 6, a semi-decoupled band, and the configurations $iA$ and $jA$ ($K^\pi = 5^+$) to Band 8.

The proposed spins for Band 6 in this work are 2 $\hbar$ lower than those previously assigned in Ref. [24]. The previous values made the moment of inertia $J^{(1)}$ of Band 6 larger than those of Bands 1 and 2, and raised its alignment curve by approximately 2 $\hbar$ in Fig. 10(c), making its aligned angular momentum larger than that of Band 1 in the region of $\hbar\omega <$ 370 keV. These considerations would make Band 6 energetically more favorable than Band 1 and thus more strongly populated, in clear contrast to the experimental results. Reducing the spins of Band 6 by 1 $\hbar$ from the previous values would also have incorrect consequences because that would alter the favored and unfavored signatures and make the more strongly populated sequence unfavored.

The spins of Band 8 are proposed so as to obtain a reasonable alignment. The uncertainty of the spin assignments is expected to be less than 2 $\hbar$. Band 8 shows an unusual signature inversion that will be discussed in Sec. IV K.

A second band crossing occurs in Bands 6 and 8 around $\hbar\omega \approx 520$ keV [see Fig. 10(c)]. The full alignment gains could not be measured, because these two bands were not observed to sufficiently high spins. However, the crossings are likely caused by the same proton $fg$ crossing as in positive-parity Band 1, considering that the bands have similar crossing frequencies and the same pattern of sharp upbending.

### I. Band 7

Band 7 has a large alignment of 15.1 $\hbar$, which is 3.4 $\hbar$ in excess of that of the ($30^+$) level of the $dABC$ configuration, to which it decays. A reasonable assumption is that the band consists of a six-quasiparticle configuration, with two more aligned neutrons. As presented in Fig. 10(c), Band 7 spans a region of rotational frequencies from 0.46 to 0.62 MeV without any sign of band crossing. This indicates that the possible proton crossings in this region, $fg$ or $ef$, are blocked. It is therefore likely that Band 7 involves the proton orbitals $e$, $f$, or $g$, in any case, an orbital other than orbital $d$. The orbitals $f$ and $g$ are lower than $e$, and more likely to be populated. A configuration involving orbital $g$, the $gABC$ sequence of Band 4, is already seen to $\hbar\omega \approx 0.57$ MeV. It would be difficult for a six-quasiparticle configuration, e.g., $gABCDE$, to survive high above configuration $gABC$, considering that the excitation energy of $gABC$ increases rapidly at the highest spins, see Fig. 11(b). These considerations indicate that the proton orbitals $e$ and $g$ are less likely candidates than $f$.

Therefore a tentative suggestion is that Band 7 may involve the proton orbital $f$, and in addition, two more aligned neutron orbitals $D$ and $E$, i.e., Band 7 may have a six-quasiparticle configuration of $fABCDE$. Such a configuration can generate the observed alignment and is consistent with the observed parity and signature. A configuration involving the proton $i_{13/2}$ intruder orbital, $\pi[660]1/2^+ \otimes ABC$, can also be ruled out since the $\pi i_{13/2}$ orbital would generate $\approx 6\hbar$ aligned angular momentum which would be too large for Band 7. This implies that Band 7 is not a TSD band since all TSD bands in the $A \approx 160$ region, whether built on the wobbling mode or on quasiparticle excitations, involve the excitation of a $\pi[660]1/2^+$ quasiproton, which drives the nucleus to large deformation at large triaxiality. This assessment is further supported by the dynamical moments of inertia $J^{(2)}$ of Band 7 (not shown in Fig. 12) whose values are similar to the average values of Band 6. Large $J^{(2)}$ values, excluding those caused by band crossings, are often an indication for bands with large deformation.

### J. Additivity of Routhians

A comparison of the experimental Routhians of two-quasiparticle bands with respect to the sum of Routhians resulting from the one-quasiparticle bands in the neighboring odd-$A$ nuclei can help to further validate the configuration assignments [44]. Figure 14 shows the experimental Routhians of two of the bands, Bands 4 and 5, in $^{168}$Lu. Routhian values were extracted before the band crossing at a rotational frequency of $\hbar\omega = 0.2$ MeV, and compared with the respective sums of average Routhian values of the neighboring odd-$Z$ ($^{167}$Lu [20] and $^{169}$Lu [29]) and odd-$N$ ($^{167}$Yb [30] and $^{169}$Hf [31]) nuclei. The Harris parameters used for $^{168}$Lu are the same throughout this work, and those for the neighboring odd-A nuclei were taken from the corresponding references.

The results of this analysis are presented in Table V. Bands 6 and 8 are floating, and so their Routhian values cannot be obtained. The lower-spin (at $\hbar\omega = 0.2$ MeV) states of signature $hB$ in Band 5 are not identified. The Routhians of Bands 1 and 2 are within 80 keV of the summed ones, suggesting that the assigned configurations are correct. The small differences are caused mainly by the residual interactions, i.e., effects not included in the mean field [44]. As mentioned before, the favored $K$ coupling of Band 1 could be discerned based on the additivity of Routhians. If the $K = 1$ coupling is assumed,

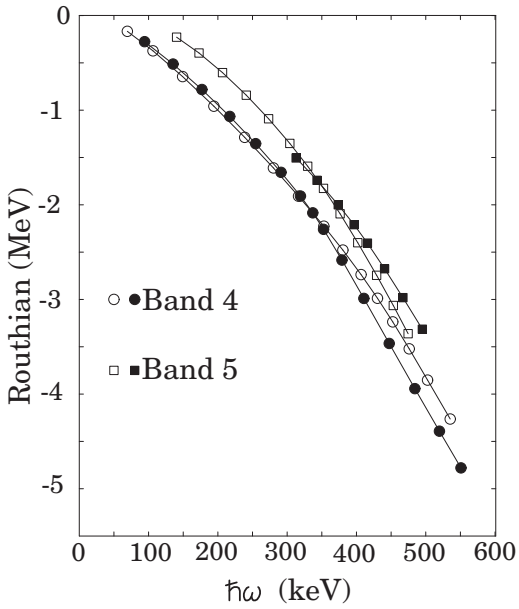


FIG. 14. Experimental Routhians of Bands 4 and 5. Open (filled) symbols represent $\alpha = 0$ ($\alpha = 1$) rotational sequences. A reference with Harris parameters $J_0 = 30\ \hbar^2\ \mathrm{MeV}^{-1}$ and $J_1 = 45\ \hbar^4\ \mathrm{MeV}^{-3}$ was subtracted from the data.

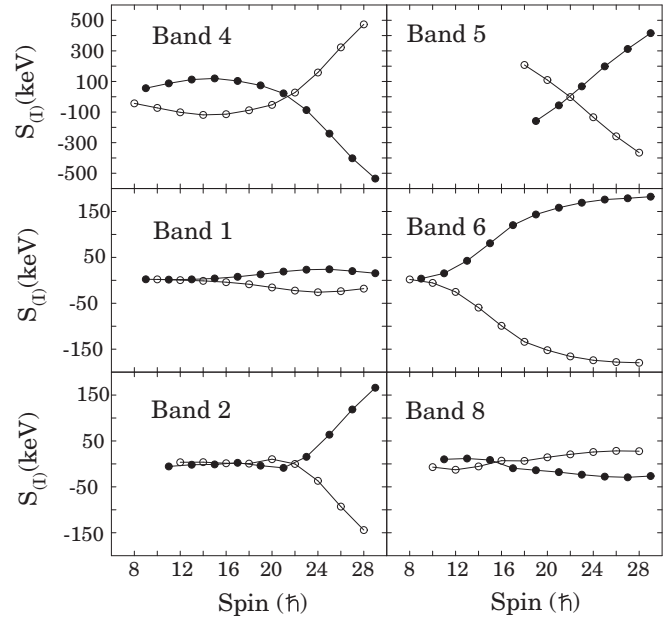


FIG. 15. Signature splitting functions for bands in $^{168}$Lu. Open symbols represent $\alpha = 0$ sequences and closed symbols $\alpha = 1$ sequences. The spins of Bands 6 and 8 are uncertain. See text for discussion.

$\delta e' = -0.22$ MeV is found. If $K = 6$ is assumed, $\delta e'$ is only 0.08 MeV. Therefore, the latter coupling is favored. The values for Bands 4 and 5 will be discussed next for signature inversion.

### K. Signature inversion

Low-spin signature inversion in doubly odd nuclei, where the predicted favored sequence is raised in energy above its partner at low spins, always attracts special attention. In the $A \approx 160$ mass region, the phenomenon has been observed in a number of nuclei for bands involving the $\pi h_{11/2} \otimes \nu i_{13/2}$ [45,46] and $\pi h_{9/2} \otimes \nu i_{13/2}$ [47] configurations. Bands 4 and 5 are associated with the latter, and both exhibit low-spin signature inversion. We consider Band 4 first.

TABLE V. Comparison of measured Routhian values $e'$ (in MeV) for bands in $^{168}$Lu with $e'_{av}$, the sum of average Routhians from neighboring odd-$Z$ and odd-$N$ nuclei, together with the difference $\delta e' = e' - e'_{av}$. The $K^\pi$ value for each band and the signature (favored/unfavored) for each configuration are also listed.

| Band | $K^\pi$ | Conf. | $\alpha$ | $e'$ | $e'_{av}$ | $\delta e'$ |
|---|---|---|---|---|---|---|
| 1 | $6^+$ | $aA$ | 1 (unf) | −0.78 | −0.86 | 0.08 |
| | | $bA$ | 0 (fav) | −0.78 | −0.86 | 0.08 |
| 2 | $7^-$ | $eA$ | 1 (unf) | −0.63 | −0.67 | 0.04 |
| | | $fA$ | 0 (fav) | −0.63 | −0.68 | 0.05 |
| 4 | $2^-$ | $gA$ | 1 (fav) | −0.95 | −1.16 | 0.21 |
| | | $gB$ | 0 (unf) | −1.00 | −1.01 | 0.01 |
| 5 | $3^-$ | $hA$ | 0 (fav) | −0.56 | −0.68 | 0.12 |
| | | $hB$ | 1 (unf) | | −0.53 | |
| 6 | $2^+$ | $cA$ | 1 (unf) | | −0.67 | |
| | | $dA$ | 0 (fav) | | −0.78 | |
| 8 | $5^+$ | $iA$ | 1 (fav) | | −0.68 | |
| | | $jA$ | 0 (unf) | | −0.68 | |

Figure 14 shows that the two signatures of Band 4 ($gA$, $gB$) cross each other. At low frequencies the favored signature $gA$ is unexpectedly ≈50 keV *higher* than the unfavored $gB$, giving signature inversion. The two signatures of Band 4 are built on the quasiproton orbital $g$ coupled to the $A$ (favored) and the $B$ (unfavored) $\nu i_{13/2}$ quasineutron orbitals. In the neighboring odd-neutron nucleus $^{167}$Yb [30], the favored signature of the $\nu i_{13/2}$ orbital is 135 keV *lower* than the unfavored at rotational frequency $\hbar\omega = 0.2$ MeV. Obviously the splitting of Band 4 does not simply reflect that of the two signatures of the $\nu i_{13/2}$ orbital.

It is customary to use the signature splitting function $S_{(I)}$ to amplify the effect graphically, where

$$S_{(I)} = E_{(I)} - E_{(I-1)} - \frac{E_{(I+1)} - E_{(I)} + E_{(I-1)} - E_{(I-2)}}{2}.$$

Figure 15 displays the $S_{(I)}$ plots for bands in $^{168}$Lu where the pronounced low-spin signature inversion in Band 4 can be seen. The measured quantities in Table V indicate that, with $\delta e' = 10$ keV, there is an excellent match between the unfavored signature ($gB$, $\alpha = 0$) and the average of the sum of the respective Routhians from neighboring odd-$Z$ and odd-$N$ nuclei. However, when a similar comparison is made for the favored signature ($gA$, $\alpha = 1$), there is a striking discrepancy. For the $gA$ sequence $\delta e' = 210$ keV, i.e., the favored signature has been shifted upward 200 keV more than the unfavored one. Thus the Routhian of the favored signature is raised above that of its unfavored partner, resulting in a signature inversion. The sign of the splitting reverts to normal above

the reversion frequency $\hbar\omega_i = 0.34$ MeV (or reversion spin $I_i = 21.7\,\hbar$), which is another useful quantity to understand the strength of forces responsible for creating the inversion. If the reversion takes place at higher frequency, the inverting force is likely to be stronger in that configuration.

Signature inversion of the $\pi h_{9/2} \otimes \nu i_{13/2}$ bands has been observed in $^{166}$Lu [48], $^{170}$Lu [49], as well as some neighboring doubly-odd Tm, Ta, Re, and Ir nuclei (see Ref. [47] and references therein). For example, the favored Routhians of the $\pi h_{9/2} \otimes \nu i_{13/2}$ bands in $^{164}$Tm [36] and $^{170}$Ta [38] were found to be raised 230 and 250 keV relative to the unfavored ones, respectively, in good agreement with our result for Band 4. The reversion spin of Band 4 is consistent with the general trend in the region where $I_i$ increases with increasing $N$ and decreases with increasing $Z$. Various explanations for signature inversion have been discussed in many papers, such as Refs. [50–53]. Among them, the particle-rotor model calculations with inclusion of residual proton-neutron ($pn$) interaction demonstrated that the $pn$ interaction is the major factor causing the signature inversion of $\pi h_{9/2} \otimes \nu i_{13/2}$ band in $^{164}$Tm [36]. The $pn$ interaction could also account for half of the delay in the $\nu i_{13/2}$ band crossing frequency. The remainder of the delay has been attributed to the increased deformation of the band. Calculations for $^{162,164}$Tm and $^{174}$Ta [53] yielded similar results.

Turning now to Band 5, Fig. 14 shows that the two signatures ($hA$, $hB$) also cross each other, indicating a signature inversion with a reversion frequency of $\hbar\omega_i = 0.35$ MeV. This is the first observation of signature inversion based on the unfavored signature of the $\pi h_{9/2}$ quasiproton orbital in the mass region. Table V shows that, just like in signature $gA$ of Band 4, there is a large (120 keV) upward shift in the favored sequence ($hA$) of Band 5 relative to the average of the sum of the respective Routhians from neighboring odd-$Z$ and odd-$N$ nuclei. A reversion spin $I_i = 22.0\,\hbar$ can be obtained from the plots of splitting function in Fig. 15.

Low-spin signature inversion is known to occur systematically for $\pi h_{11/2} \otimes \nu i_{13/2}$ bands in this mass region, and the magnitude of the inversion decreases with increasing $N$ for a chain of isotopes. This is, indeed, the trend seen in $^{162,164,166}$Lu [46], and the inversion disappears in Band 2 of $^{168}$Lu. Even though the $S_{(I)}$ values of a few data points in the favored signature $fA$ of Band 2 are slightly higher (<5 keV) than those of $eA$, as shown in Fig. 15, no inversion or signature splitting is clearly defined below spin 22.

The signature splitting in Band 8 is also small ($S_{(I)} < 30$ keV), as expected for a strongly coupled band. However, there exists a small signature inversion ($S_{(I)} \leqslant 12$ keV) with a reversion spin $I_i = 15.4\,\hbar$. Similar small inversion has been reported in two cases for $\pi[411]1/2^+ \otimes \nu[642]5/2^+$ bands, $I_i = 9\,\hbar$ in $^{164}$Tm [36] and $I_i = 10\,\hbar$ in $^{166}$Tm [37], but not for any $\pi[402]5/2^+ \otimes \nu[642]5/2^+$ band in this region. There is no systematic study for these small inversions since only a few separate cases have been observed. It is not uncommon to see a band built on $\pi[402]5/2^+$ mix with one built on the $\pi[411]1/2^+$ Nilsson orbital, which may introduce additional complication to a detailed investigation of these small signature inversions, as well as the signature splittings.

The signature splitting of Band 6 is considerably larger than those of the three strongly coupled bands, Bands 1, 2, and 8 (see Fig. 15). This is consistent with the suggested configuration of $\pi[411]1/2^+ \otimes \nu[642]5/2^+$ for Band 6 as a semidecoupled band. It is also expected from the systematics of neighboring nuclei, as seen in Table V, the average Routhian of the favored signature $dA$ is 110 keV lower than that of $cA$.

## V. SUMMARY

This work presents an extensive high-spin spectroscopic study of the odd-odd nucleus $^{168}$Lu. It confirmed the previously known bands (Bands 1–4 and 6), and three new bands were identified: Bands 5, 7, and 8. All but two bands now have been connected to each other. The level scheme was extended to spins as high as 50 $\hbar$. The data suggests that Band 5 is built on the unfavored signature $h$ of the $\pi h_{9/2}$ orbital, coupled to the $A$ and $B$ quasineutrons. The configuration of Band 6 was reassigned as $\pi d_{3/2} \otimes \nu i_{13/2}$. The strongly coupled Band 8 is assigned the configuration $\pi d_{5/2} \otimes \nu i_{13/2}$.

The first band crossing in all of the main bands are attributed to the $BC$ neutron alignment, except for the unfavored sequences $gB$ and $hB$ in Bands 4 and 5, respectively, where the $AD$ neutron alignment is suggested. Three positive parity bands, Bands 1, 6, and 8, exhibit a second band crossing, attaining a six-quasiparticle configuration at the highest spins, associated with a hybrid $fg$ proton crossing. Band 7, a single sequence of $E2$ decays, is tentatively assigned the six-quasiparticle configuration $fABCDE$. On the negative-parity side, the proton $ef$ and $fg$ crossings are blocked for the two signatures of Band 2 and the second crossing around $\hbar\omega = 0.63$ MeV in the $fA$ sequence has been associated with a $EF$ neutron crossing. For Bands 4 and 5, the higher crossings are delayed due to the larger deformation of the bands, and are not observed in our data.

Low-spin signature inversions are observed in Bands 4 and 5. This is consistent with a systematic trend of such anomalous splitting for the $\pi h_{9/2} \otimes \nu i_{13/2}$ bands in the region, presumably caused by a residual $pn$ interaction. In Band 4, the Routhians of its favored signature $gA$ is raised by 210 keV at $\hbar\omega = 0.2$ MeV. Band 5 is the first case where the signature inversion is observed in a band built on the unfavored signature $h$ of the $\pi h_{9/2}$ orbital. A small signature inversion is also evident in Band 8 which is unexpected on the basis of systematics.

After an extensive band search, no evidence is found for triaxial strongly deformed structures as predicted by cranking calculations employing the ULTIMATE CRANKER code.

## ACKNOWLEDGMENTS

We thank the staff of the Berkeley Cyclotron for providing the beams and we greatly appreciate the support obtained from A. O. Macchiavelli and the staff involved in running the Gammasphere spectrometer. This research was supported by the U.S. Department of Energy, Office of Science, Office of Nuclear Physics, under Award No. DE-FG02-95ER40939 (MSU) and under Contract No. DE-

AC03-76SF00098 (LBNL), the Danish Science Foundation, and the German BMBF under Grants No. 06 BN 907 and No. 06 BN 109. D.G.R. and W.C.M. thank NBI for partial support during their visits.


[1] A. Bohr and B. R. Mottleson, *Nuclear Structure*, Vol. II (Benjamin, New York, 1975).

[2] S. W. Ødegård, G. B. Hagemann, D. R. Jensen, M. Bergström, B. Herskind, G. Sletten, S. Tormanen, J. N. Wilson, P. O. Tjom, I. Hamamoto, K. Spohr, H. Hubel, A. Gorgen, G. Schonwasser, A. Bracco, S. Leoni, A. Maj, C. M. Petrache, P. Bednarczyk, and D. Curien, Phys. Rev. Lett. **86**, 5866 (2001).

[3] D. R. Jensen, G. B. Hagemann, I. Hamamoto, S. W. Ødegård, B. Herskind, G. Sletten, J. N. Wilson, K. Spohr, H. Hubel, P. Bringel, A. Neusser, G. Schonwasser, A. K. Singh, W. C. Ma, H. Amro, A. Bracco, S. Leoni, G. Benzoni, A. Maj, C. M. Petrache, G. LoBianco, P. Bednarczyk, and D. Curien, Phys. Rev. Lett. **89**, 142503 (2002).

[4] G. Schönwaßer, H. Hübel, G. B. Hagemann, P. Bednarczyk, G. Benzoni, A. Bracco *et al.*, Phys. Lett. B **552**, 9 (2003).

[5] H. Amro, W. C. Ma, G. B. Hagemann, R. M. Diamond, J. Domscheit, P. Fallon *et al.*, Phys. Lett. B **553**, 197 (2003).

[6] P. Bringel, G. B. Hagemann, H. Hübel, A. Al-khatib, P. Bednarczyk, A. Bürger*et al.*, Eur. Phys. J. A **24**, 167 (2005).

[7] D. J. Hartley, R. V. F. Janssens, L. L. Riedinger, M. A. Riley, A. Aguilar, M. P. Carpenter *et al.*, Phys. Rev. C **80**, 041304(R) (2009).

[8] D. R. Jensen, G. B. Hagemann, I. Hamamoto, B. Herskind, G. Sletten, J. N. Wilson *et al.*, Eur. Phys. J. A **19**, 173 (2004).

[9] P. Bringel, C. Engelhardt, H. Hübel, A. Neußer-Neffgen, S. W. Ødegård, G. B. Hagemann, C. R. Hansen, B. Herskind, G. Sletten, M. P. Carpenter, R. V. F. Janssens, T. L. Khoo, T. Lauritsen, D. Seweryniak, W. C. Ma, D. G. Roux, and P. Chowdhury, Phys. Rev. C **75**, 044306 (2007).

[10] J. Timár, Q. B. Chen, B. Kruzsicz, D. Sohler, I. Kuti, S. Q. Zhang *et al.*, Phys. Rev. Lett. **122**, 062501 (2019).

[11] J. T. Matta, U. Garg, W. Li, S. Frauendorf, A. D. Ayangeakaa, D. Patel *et al.*, Phys. Rev. Lett. **114**, 082501 (2015).

[12] N. Sensharma, U. Garg, S. Zhu, A. D. Ayangeakaa, S. Frauendorf, W. Li *et al.*, Phys. Lett. B **792**, 170 (2019).

[13] N. Sensharma, U. Garg, Q. B. Chen, S. Frauendorf, D. P. Burdette, J. L. Cozzi *et al.*, Phys. Rev. Lett. **124**, 052501 (2020).

[14] T. Bengtsson, Nucl. Phys. A **496**, 56 (1989).

[15] T. Bengtsson, Nucl. Phys. A **512**, 124 (1990).

[16] www.matfys.lth.se/staff/Ragnar.Bengtsson/TSD.html.

[17] H. Schnack-Peterson, R. Bengtsson, R. A. Bark, P. Bosetti, A. Brockstedt, H. Carlsson *et al.*, Nucl. Phys. A **594**, 175 (1995).

[18] R. Bengtsson and H. Ryde, Eur. Phys. J. A **22**, 355 (2004).

[19] I. Y. Lee, Nucl. Phys. A **520**, c641 (1990).

[20] D. G. Roux, W. C. Ma, G. B. Hagemann, H. Amro, D. R. Elema, P. Fallon *et al.*, Phys. Rev. C **92**, 064313 (2015).

[21] D. C. Radford, Nucl. Instrum. Methods A **361**, 297 (1995).

[22] K. S. Krane, R. M. Steffen, and R. M. Wheeler, Nucl. Data Tables **11**, 351 (1973).

[23] R. B. Yadav, W. C. Ma, G. B. Hagemann, H. Amro, A. Bracco, M. P. Carpenter *et al.*, Phys. Rev. C **80**, 064306 (2009).

[24] J. H. Ha, J. C. Kim, C. S. Lee, J. H. Lee, J. Y. Huh, C.-B. Moon *et al.*, J. Phys. Soc. Japan **71**, 1663 (2002).

[25] S. K. Katoch, S. L. Gupta, S. C. Pancholi, D. Mehta, S. Malik, G. Shanker, L. Chaturvedi, and R. K. Bhowmik, Eur. Phys. J. A **4**, 307 (1999).

[26] G. Zhao, Y. Liu, Y. Ma, X. Li, J. Lu, L. Zhu, X. Wu, G. Li, S. Wen, and C. Yang, J. Jilin Univ. (Sci. Ed.) **1**, 118 (2010).

[27] A. Charvet, R. Chery, D. H. Phuoc, R. Duffait, A. Emsallem, and G. Marguier, Nucl. Phys. A **197**, 490 (1972).

[28] V. Barci, G. Ardisson, D. Trubert, and M. Hussonnois, Phys. Rev. C **55**, 2279 (1997).

[29] S. Ogaza, J. Kownacki, M. P. Carpenter, J. Gascon, G. B. Hagemann, Y. Iwata *et al.*, Nucl. Phys. A **559**, 100 (1993).

[30] A. Fitzpatrick, S. Y. Araddad, R. Chapman, J. Copnell, F. Lidén, J. C. Lisle *et al.*, Nucl. Phys. A **582**, 335 (1995).

[31] K. A. Schmidt, M. Bergström, G. B. Hagemann, B. Herskind, G. Sletten, P. G. Varmette *et al.*, Eur. Phys. J. A **12**, 15 (2001).

[32] F. Dönau, Nucl. Phys. A **471**, 469 (1987).

[33] D. R. Jensen, J. Domscheit, G. B. Hagemann, M. Bergström, B. Herskind, B. S. Nielsen *et al.*, Eur. Phys. J. A **8**, 165 (2000).

[34] B. E. Chi, Nucl. Phys. A **83**, 97 (1966).

[35] C. J. Gallagher, Jr. and S. A. Moszkowski, Phys. Rev. **111**, 1282 (1958).

[36] W. Reviol, L. L. Riedinger, X. Z. Wang, J.-Y. Zhang, H. J. Jensen, G. B. Hagemann *et al.*, Phys. Rev. C **59**, 1351 (1999).

[37] M. A. Cardona, D. Hojman, M. E. Debray, A. J. Kreiner, M. Davidson, J. Davidson *et al.*, Phys. Rev. C **66**, 044308 (2002).

[38] A. Aguilar, D. J. Hartley, M. A. Riley, C. Teal, M. P. Carpenter, P. Chowdhury *et al.*, Phys. Rev. C **81**, 064317 (2010).

[39] G. Schönwaßer, N. Nenoff, H. Hübel, G. B. Hagemann, P. Bednarczyk, G. Benzoni *et al.*, Nucl. Phys. A **735**, 393 (2004).

[40] H. J. Jensen, R. A. Bark, P. O. Tjøm, G. B. Hagemann, I. G. Bearden, H. Carlsson *et al.*, Nucl. Phys. A **695**, 3 (2001).

[41] M. Cromaz, J. DeGraaf, T. E. Drake, D. Ward, A. Galindo-Uribarri, V. P. Janzen *et al.*, Phys. Rev. C **59**, 2406 (1999).

[42] M. B. Smith, G. J. Campbell, R. Chapman, P. O. Tjøm, R. A. Bark, G. B. Hagemann, N. Keeley, D. J. Middleton, H. Ryde, and K. M. Spohr, Eur. Phys. J. A **6**, 37 (1999).

[43] X.-H. Wang, C.-H. Yu, D. M. Cullen, D. C. Bryan, M. Devlin, M. J. Fitch *et al.*, Nucl. Phys. A **608**, 77 (1996).

[44] S. Frauendorf, L. L. Riedinger, J. D. Garrett, J. J. Gaardhøje, G. B. Hagemann, and B. Herskind, Nucl. Phys. A **431**, 511 (1984).

[45] G. García Bermúdez and M. A. Cardona, Phys. Rev. C **64**, 034311 (2001).

[46] D. J. Hartley, R. V. F. Janssens, L. L. Riedinger, M. A. Riley, X. Wang, S. L. Miller *et al.*, Phys. Rev. C **94**, 054329 (2016).

[47] Y. H. Zhang, M. Oshima, Y. Toh, X. H. Zhou, M. Koizumi, A. Osa *et al.*, Phys. Rev. C **68**, 054313 (2003).

[48] G. Zhao, Y. Liu, J. Lu, Y. Ma, L. Yin, X. Li *et al.*, Eur. Phys. J. A **9**, 299 (2000).

[49] G. Levinton, A. J. Kreiner, M. A. Cardona, M. E. Debray, D. Hojman, J. Davidson *et al.*, Phys. Rev. C **60**, 044309 (1999).

[50] R. Bengtsson, J. A. Pinston, D. Barneoud, E. Monnand, and F. Schussler, Nucl. Phys A **389**, 158 (1982).

[51] I. Hamamoto, Phys. Lett. B **235**, 221 (1990).

[52] K. Hara and Y. Sun, Nucl. Phys. A **531**, 221 (1991).

[53] R. A. Bark, J. M. Espino, W. Reviol, P. B. Semmes, H. Carlsson, I. G. Bearden *et al.*, Phys. Lett. B **406**, 193 (1997).